이학박사 학위논문

Discovery of bioactive small molecules and comprehension of its mode of action via cellular imaging

생리활성 저분자 화합물의 발굴과 세포 이미징을 통한 작용 기전의 이해

2019년 2월

서울대학교 대학원

생물물리 및 화학생물학과 화학생물학 전공

정 진 주

Discovery of bioactive small molecules and comprehension of its mode of action via cellular imaging

지도 교수 박 승 범

이 논문을 이학박사 학위논문으로 제출함

2018 년 11 월

서울대학교 대학원

생물물리 및 화학생물학과 화학생물학 전공

정 진 주

정진주의 이학박사 학위논문을 인준함

2018 년 12 월

위 원 장 _____ **(인)**

부위원장 _____ **(인)**

위 원 _____ **(인)**

위 원 _____ **(인)**

위 원 _____ **(인)**

Abstract

Discovery of bioactive small molecules and comprehension of its mode of action via cellular imaging

Jung Jinjoo

Chemical Biology major

Department of Biophysics and Chemical Biology

Seoul National University

Our body has very sophisticated and complex signaling pathways to maintain homeostasis. Therefore, we could understand growth processes based on the knowledge from researches on biological events and improve the quality of life by the suggestion of disease treatment strategies. Among various approaches to understand new biological events, the chemical biology approaches were used in this researches, especially, discovery of bioactive small molecules and visualization of its mode of action by cellular fluorescence imaging for understanding biological phenomena with various aspects.

Two biological systems were covered in this dissertation. First, studies about mechanistic target of Rapamycin complex 1 (mTORC1) regulation via Leucyl-tRNA Synthetase (LRS) and Ras-like GTPase D (RagD) protein-protein interaction was described. Three distinct

bioactive small molecules were identified by using target-based screening. New aspects on mTORC1 regulation mechanism via LRS-RagD interaction were inferred from the unique activity patterns and biophysical studies of each molecule. Second, the investigation of lipid droplet (LD) reduction mechanism was explained. To identify LD reducing small molecule, image-based LD-monitoring high-contents screening was carried out and the novel LD reduction mechanism study of the hit compound was described.

As researches on both mTORC1 regulation via LRS-RagD interaction and LD reduction mechanism are relatively deficient, new results described in this dissertation has greatly contributed to the academic field. Furthermore, it has been confirmed that it is possible to suggest a new disease treatment strategy based on the newly discovered results. Therefore, it is expected to be applied to the medicinal industry as an anti-cancer drug sensitizer and a steatosis attenuating agent.

Keyword: Chemical biology, Bioactive small molecule, Comprehension of mode of action, Cellular imaging, LRS-RagD interaction, Lipid droplet

Student Number: 2012-23917

Table of Contents

List of Figures

List of Table

Chapter 1. Introduction

1.1. Chemical biology approaches for the comprehension of new biological phenomena

It is important to understand biological phenomena. Advanced knowledge about biological phenomena satisfies scientist's curiosity academically and makes it possible to develop new therapeutics based on the comprehension in the industrial field. However, it is not easy to clearly understand molecular mechanisms. In chemical biology field, various researches and efforts are currently underway to explain the mysteries of biological systems with chemical tools and terms. In this dissertation, I make advances to explain the research using bioactive small molecules and cellular fluorescence imaging.

1.1.1. Discovery of bioactive small molecules

Bioactive small molecules perturbed biological systems give us hints to solve problems or discover unfound mechanisms. The discovery of a smart bioactive small molecule is connected to the comprehension of a novel mechanism by its mode of action exploration. There are two approaches to discover a new bioactive small molecule, target-based approach and phenotype-based approach (Fig. 1.1) [1-3]. Target-based

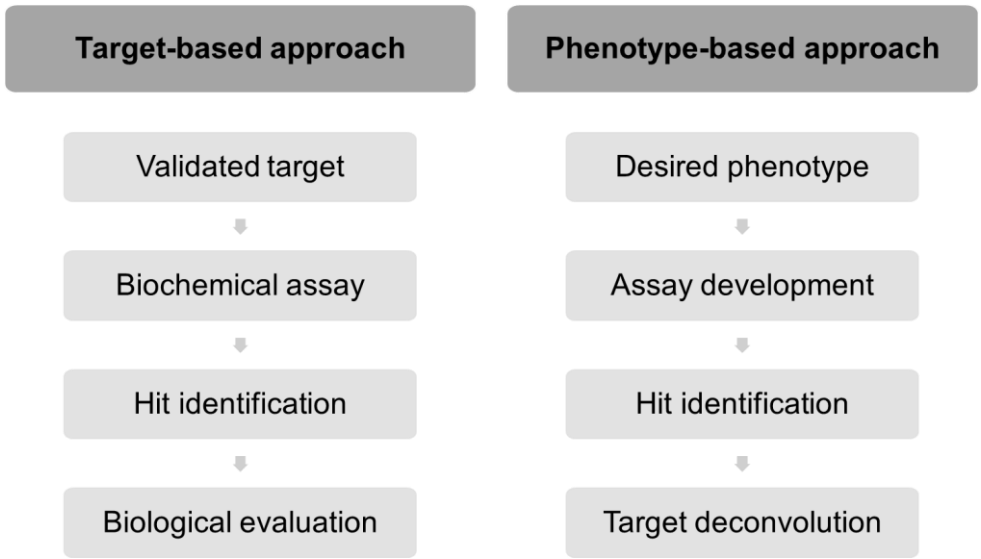

Figure 1.1. Target-based approach and phenotype-based approach

approach starts with the selection of validated target molecules. A proper assay system is designed and followed by screening small molecule library with high-throughput manner. A representative target-based screening is an enzymatic assay or reporter gene assay. This approach has advantages of known target molecules, known mechanism of action and, therefore, ability to measure direct effects on targets but targeting strategy could not give desired results and it may have off-target effects.

Unlike the target-based approach, phenotype-based approach focuses on the final outcomes of signaling pathways from multiple interconnected pathways as the changes in disease-relevant phenotypes [3, 4]. For phenotypic-based approach, screening system which enables the monitoring of interested phonotype is needed. A typical phonotype-based screening is a cellular assay with which cell

proliferation or cell death is observed. The weakness of this approach is unknown target molecule. The identification of target molecule and mode of action can be quite challenging. However, because bioactive small molecules selected from phonotype-based screening are from intact biological system, it is possible to have multiple targets and/or mechanisms of action, given new information to knowledge-deficient biological events.

Recent advances in automated imaging technology involving the use of multi-well plates and automated image analysis ensure the robust and rapid screening of a large collection of small molecule libraries with image-based high throughput screening. Moreover, fluorescence technology now allows high-throughput imaging with multiple channels with an excellent signal-to-noise ratio. Therefore, a lot of information about phenotypic changes can be extracted from a single experiment, and this information can then be analyzed to evaluate the potential of the compounds [4]. The one of the excellent system which is monitoring LD with a specific LD staining fluorescent dye, SF44, in image-based high-throughput manner was developed in Park's group [5, 6].

1.1.2. Cellular Imaging

Fluorescence is an optical phenomenon in which the molecular absorption of energy in the form of photons triggers the emission of

fluorescent photons with a longer wavelength [7]. As more sophisticated microscope and camera have been improved and various fluorescent dyes and fluorescent proteins have been developed, it has been allowed to get high-resolution fluorescent images of fluorescence tagged or stained biomolecules in biological systems. Therefore, a lot of information which cannot be obtained from proteomics studies is acquired with proper fluorescent molecules easily and fast. For example, cellular fluorescence imaging comes across with spatial information of specific molecules such as specific location or distribution. In addition, functional or structural interaction partners can be confirmed.

Nowadays, time-lapse imaging in live cell condition is possible and it allows to study molecular dynamics. This skill is well applicable to observe protein-protein interaction (PPI) in cell. To study PPI, there are many approaches including FP (fluorescence polarization), ELISA (enzyme-linked immunosorbent assay) and FRET (fluorescence resonance electron transfer) [8].

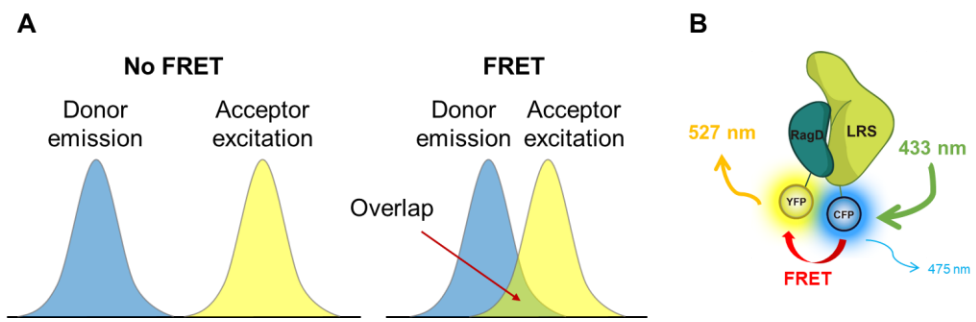

Figure 1.2. FRET (A) Schematic diagrams depicting the condition for efficient FRET. The energy of donor emission must be an energy that the acceptor can absorb. (B) one application example of FRET to cellular imaging

In this dissertation, I would like to focus on FRET phenomena (Fig. 1.2A). FRET phenomenon is one of photo-physical mechanism describing photon energy transfer from one light-exited molecule, a donor, to another light-acceptable molecule, an acceptor, and emits a virtual photon with longer wavelength [9, 10]. FRET phenomenon is very sensitive to distance between the donor and the acceptor, therefore, it is used for studying PPI.

FRET phenomenon is distinct from FP and ELISA as it can be applied to cellular imaging [11] with expression of two interaction molecule pair tagged with each fluorescent molecules in live cell. Other methods are carried out in vitro and confirm only end point. However, by applying FRET to cellular imaging (Fig. 1.2B), dynamic process besides end point results can be monitored with time-lapse monitoring.

1.2. mTORC1 pathway and LRS-RagD interaction

Mechanistic target of Rapamycin (mTOR) which is a highly conserved serine/threonine kinase and it acts a key integrator of environmental cues such as glucose, amino acid and growth factor availability [12, 13]. Thus, we can understand how our body grows through the research about mTOR signaling pathway.

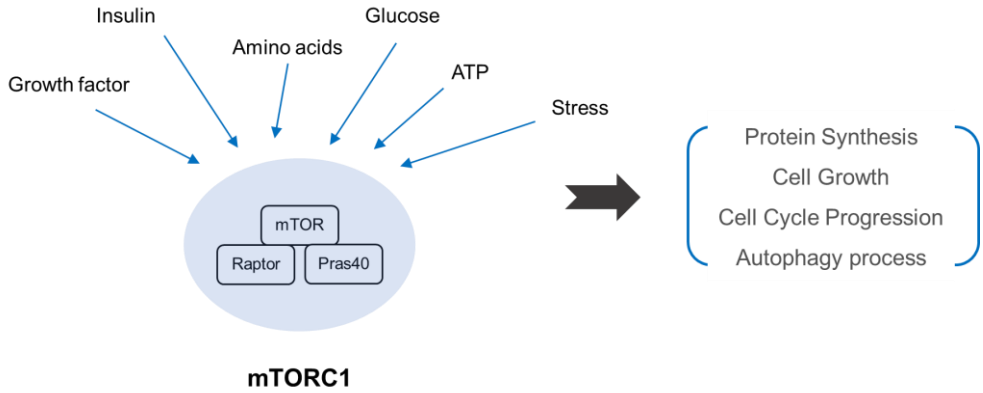

Figure 1.3. Various environmental cues to activate mTORC1 and regulated phenotypes under mTORC1

mTOR exists in two functionally and structurally distinct complexes, mTOR complex 1 (mTORC1) and mTORC2. mTORC1 is composed of mTOR, RAPTOR (regulatory-associated protein of mTOR), mLST8 (mammalian lethal with SEC thirteen 8) and the recently identified PRAS40 and DEPTOR whereas, those of mTORC2 are mTOR, RICTOR (rapamycin-insensitive companion of mTOR), SIN1 (SAPK-interacting 1) and mLST8.

mTORC1 responds to amino acids, stress, oxygen, energy, and growth factors (Fig. 1.3) and is acutely sensitive to rapamycin which binds to 12-kDa FK506-binding protein (FPBP12) and disrupts integration of mTOR complex [14]. Under nutrient-rich conditions, mTORC1 promotes cell growth and proliferation by stimulating biosynthetic pathways, including mRNA transcription and translation, and by inhibiting cellular catabolism through repression of the autophagy pathway and also drives cell-cycle progression. mTORC2 responds to growth factors and regulates cell survival and metabolism,

as well as the cytoskeleton [15, 16]. mTORC2 is insensitive to acute rapamycin treatment but chronic exposure to the drug can disrupt its structure.

mTORC1 is highly considered to therapeutic target [17-19] because of its activation in many diseases, especially cancers. As shown in Fig. 1.4, many oncogenic proteins or tumor suppressor proteins are engaged in mTORC1 signaling pathway [13]. Cancer cells make mTORC1 excitable status by overactivating of oncogenic proteins or losing of tumor suppressor proteins and they finally make mTORC1 unsleeping factory to grow or proliferate itself by increasing protein translation and lipid synthesis. Therefore, the dysregulation of mTORC1 activation could lead to malfunction in central biological

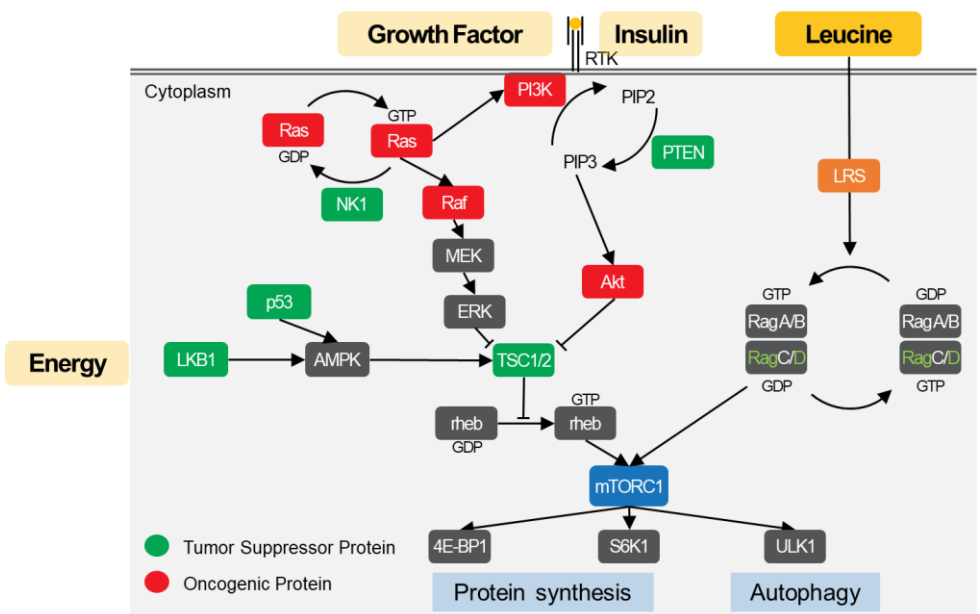

Figure 1.4. The key signaling nodes that regulate mTORC1. In this figure, the proteins depicted in red are oncogenes, and the ones in green are tumor suppressors.

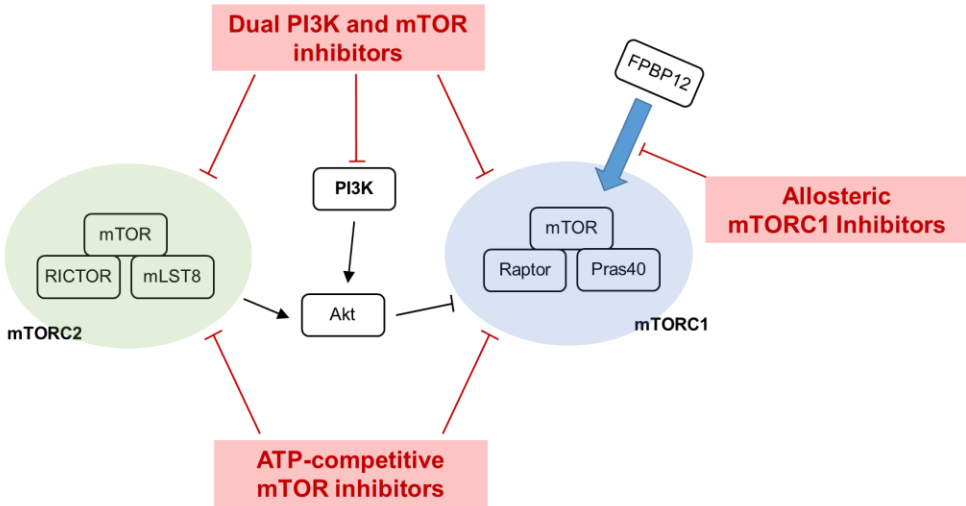

Figure 1.5. The three classes of mammalian target of rapamycin (mTOR) inhibitors.

pathways that could lead to cancer cell growth, survival and proliferation and makes it an attractive therapeutic target in drug discovery research.

There are three conventional approaches for targeting mTORC1 (Fig. 1.5) [20, 21]. First, allosteric mTOR inhibitors such as rapamycin and rapalogs have been developed. It associates with FKBP12, leading to dissociate Raptor from mTORC1 and to block mTORC1 formation. This approach is the most common way to develop an mTORC1 inhibitor but it has Rapamycin resistance, that is, Rapamycin cannot affect as an anti-cancer drugs in some cancer and negative feedback to Akt signaling pathway is also a big considerable problem [22]. Second, there are covalent inhibitors such as dual PI3K/mTOR inhibitors or ATP-competitive inhibitors. Dual

PI3K/mTOR inhibitors target both PI3K and mTORC1/mTORC2, acting on the catalytic sites of PI3K and mTOR and ATP-competitive mTORC1/mTORC2 inhibitors specifically target the catalytic site of mTOR. It is expected these approaches show more powerful effects to cancer but these inhibitors also have resistance. To overcome the resistance, researchers have been working until nowadays but it is not a simple problem because it is difficult to confirm the compound's activity before clinical trial because there is no biomarker to determine resistance. As a novel mode of action to target mTORC1, mTORC1 pathway via amino acid sensing which is different from conventional ways targeting PI3K signaling or mTORC1 itself is focused on.

Amino acids are essential nutrients to stimulate mTORC1 signaling and process for protein synthesis [16, 23, 24]. Among essential amino acids, Leucine, arginine and glutamine are implicated in mTORC1 activation [25] and especially, leucine is the most potent amino acid for that [26, 27]. There is now strong evidence that leucine represses proteasomal degradation as well as enhancing mTORC1 signaling to promote growth [28, 29]. Though the importance of leucine mediated mTORC1 signaling, limited information about the mechanism had been oppressive. Since the first paper about an mTORC1 activation in an amino acid dependent manner was published in 2012, the amino acid sensing mechanism comes to the front and have studied vigorously [30-35].

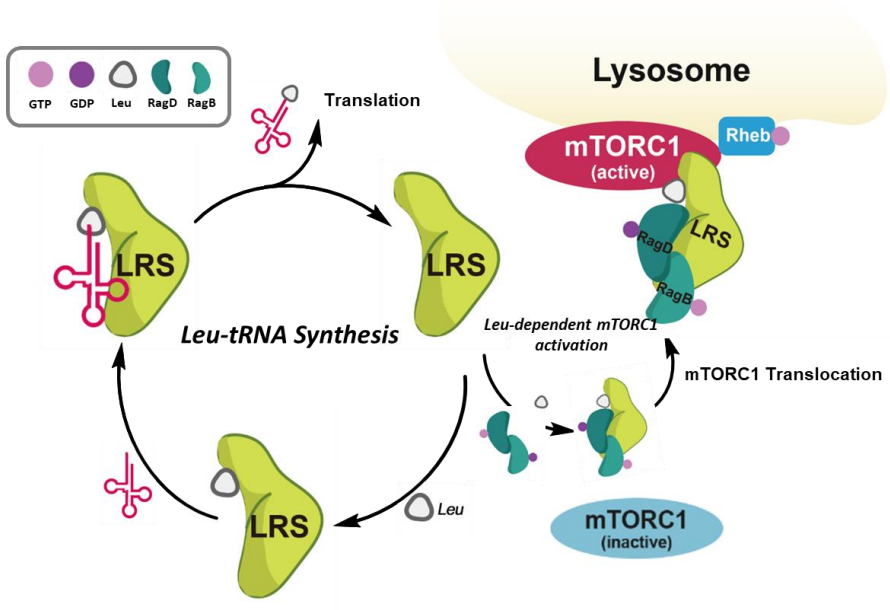

Figure 1.6. Roles of leucyl-tRNA synthetase. (i) Canonical role (left circle) of leucyl-tRNA synthetase; LRS conjugates leucine and cognate tRNA. (ii) Non-canonical role (right circle) of LRS–leucine-dependent mTORC1 activation; LRS binds to RagD and activates mTORC1 in a leucine-dependent manner

One of the most remarkable mechanism is Leucyl-tRNA synthetase (LRS) and Ras-like GTPase D (RagD) interaction (Fig. 1.6). LRS has a canonical role to catalyze the conjugation of leucine (Leu) to its cognate tRNA to form an aminoacyl-tRNA, which serves as a precursor for protein synthesis. In 2012, Kim's group reported that a noncanonical role of LRS in amino acid-dependent mTORC1 activation [30]. According to this study, LRS can sense and charge Leu to activate mTORC1 and binds to RagD-GTP protein to form a LRS–RagD protein complex in a Leu-dependent manner, which leads to translocate mTORC1 to the lysosome membrane and subsequent

activation of mTORC1. Thus, LRS–RagD interaction could serve as a Leu-sensing mechanism in the amino acid-dependent activation of mTORC1.

1.3. Lipid droplet and autophagy

Lipid is one of the important nutrients in our body. Lipids are degraded into free fatty acids in intestine and absorbed free fatty acids go to cells. Lipid droplet (called LD) is a specialized organelle used for cellular free fatty acid storage as a neutral lipid form such as triacylglycerol or sterol esters [36, 37].

Neutral lipids are surrounded with phospholipids and some surface proteins such as perillipin families and lipases [37]. This well-shaped organelle can make itself store lipid efficient manner and avoid lipotoxicity of free fatty acid. Recently, in addition to its basic functions, other functions of LD have been reported such as transcription factors or chromatin components sequestration, lipid ligands generation for certain nuclear receptors and synthesis immune related proteins for host defense [38, 39].

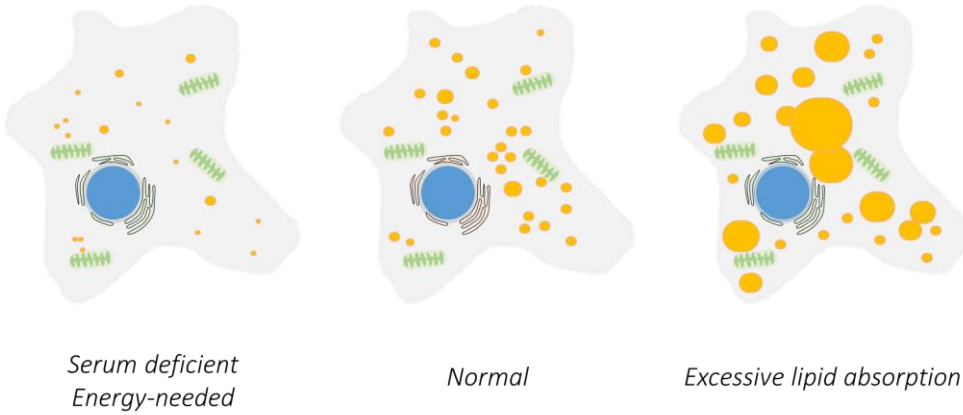

Figure 1.7. LD as a dynamic organelle. LD changes its form depending on its energy condition.

LD is very dynamic organelle which can change its forms over their environment such as tissue types and energy conditions. When adipose cells absorb too much fats, LD stores free fatty acid as much as possible and make itself big. The other way, in starved condition, stored lipids may be used for membrane components and energy sources needed and the number and size of LD are reduced (Fig. 1.7). Therefore, LD plays an important role in energy homeostasis and lipid metabolisms.

LD *de novo* formation occurs from the endoplasmic reticulum (ER) membrane generally [39-41]. First, neutral lipid synthesized in the ER and accumulate within the bilayer. And, once the local concentration of neutral lipid reaches a crucial threshold, a lens will form. As the lens accumulates additional neutral lipids, the bilayer deforms and a nascent lipid droplet buds into the cytoplasm. The nascent droplet might remain attached to the ER or separate completely.

For degradation of LD, cell uses classic two mechanisms [40, 42, 43], neutral lipolysis via lipases (Fig. 1.8) and acidic lipolysis via autophagy-lysosome system (Fig. 1.9). First, neutral lipolysis is mediated by some lipases on LD surface. Adipose triglyceride lipase, called ATGL, hormone sensitive lipase, HSL and monoacylglycerol lipase, MGL hydrolyses TG, DAG and MAG in order and finally

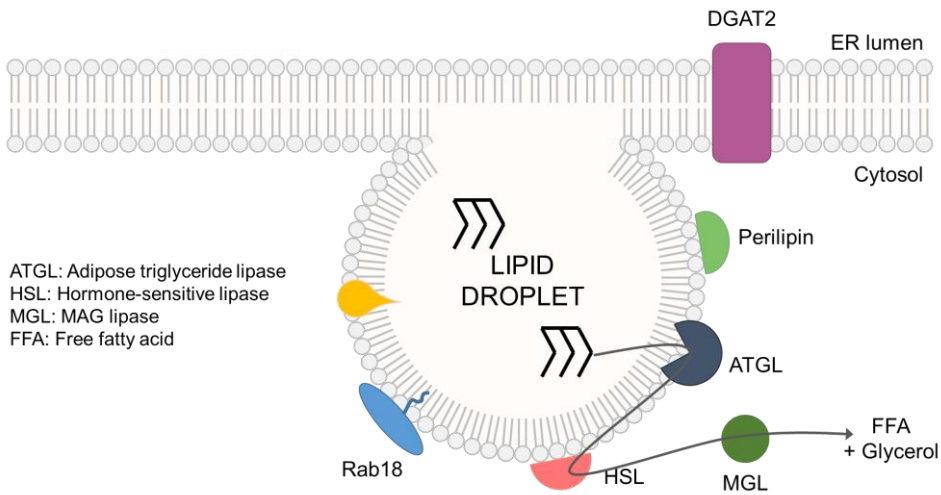

Figure 1.8. LD clearance mechanism by lipases

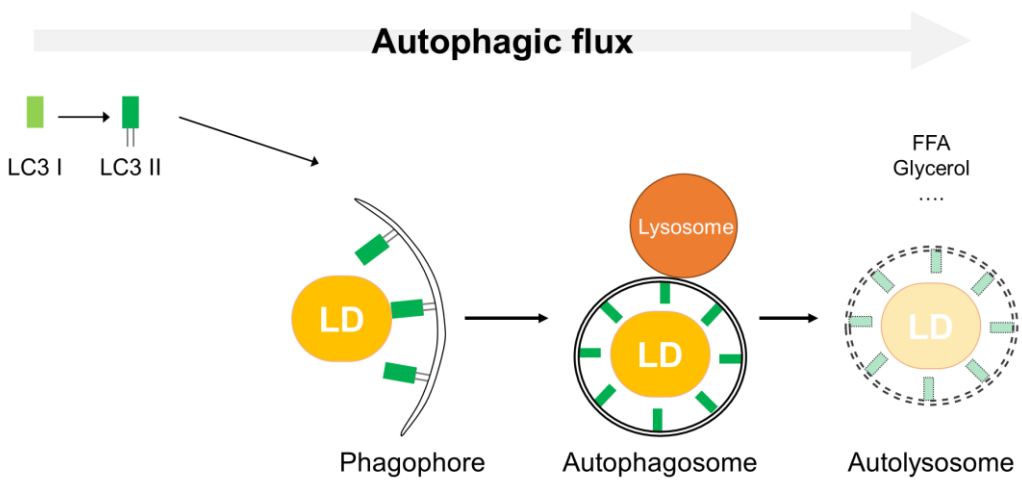

Figure 1.9 LD clearance mechanism by autophagy process

released free fatty acid and glycerol.

Second, LD can be broken through autophagy process [44]. In order to maintain cell homeostasis, a balance between anabolic and catabolic processes is crucial. Autophagy is the major catabolic process for the turnover of proteins and organelles in cellular systems [45, 46]. As inferred from its Greek origin, autophagy is self-destructive process of cytoplasmic biomolecules. The eukaryotic cell has adapted the autophagy process evolutionally to cope with starvation condition. Deficient nutrients are obtained by degrading cytoplasmic components randomly through autophagy process. The process of autophagy starts with the formation of a double membrane organelle known as the autophagosome, which engulfs cytoplasmic materials and eventually sequesters them from the cytosol into a vesicle. Next, the autophagosome fuses with a lysosome to form an autolysosome, which enables the degradation of the contained materials for the recycling process.

Recently, specific cellular organelles also have been described as substrates of autophagy [47, 48]. In this cases, damaged organelles are sequestrated into autophagosome to break up. This process is substrate selective process so it is called selective autophagy, for example, mitophagy (mitochondria) [49], pexophagy (peroxisome) [50], ribophagy (ribosome), xenophagy (invading pathogen). LD is also known as a selective autophagy substrate (lipophagy) [44, 51, 52].

As a key mediator for selective autophagy, the ubiquitination of

substrates has been demonstrated [50, 53]. Ubiquitination is the addition of ubiquitin protein to a lysine residue on the substrate protein. Ubiquitination is generally used to mark the unnecessary proteins such as misfolded or damaged proteins for degrading by proteasomes. This process is mediated by three types of enzymes, ubiquitin-activating enzymes, ubiquitin-conjugating enzymes, and ubiquitin ligases, known as E1s, E2s, and E3s, respectively. The ubiquitin is activated by an E1 with ATP dependent manner to make thioester linkage between the ubiquitin and E1 and E2 catalyzes ubiquitin transfer from E1 to the active site cysteine of the E2. E3 recognizes the substrate specifically and finally connects ubiquitin and substrate by binding E2-ubiquitin complex. Generally, the ubiquitinated substrates are degraded by the proteasome. In the ubiquitination cascade, E1 can bind with many E2s, which can bind with hundreds of E3s in a hierarchical way.

For selective autophagy, some cargo receptors including SQSTM1 [54, 55], NBR1 and OPTN have been reported as ubiquitin-binding proteins that mediate the interaction between ubiquitinated substrates and the autophagy machinery.

Since LD comes out into the open, many biological mechanisms are identified, however, more specific studies are necessary because the basic LD regulating mechanisms have not even defined in details. Furthermore, LD research field have been emerged as a major interest because of its importance in biological and physiological systems

though its limited information and research pools. The relationship between LD and metabolic diseases has been closed each other [52]. Accumulation of LD in muscle, liver tissue goes as far as to be considered as a hallmark of metabolic diseases such as type 2 diabetes, obesity and atherosclerosis [56, 57].

1.4. Aims of the dissertation

In this dissertation, I describe the research using bioactive small molecules and cellular fluorescence imaging to understand biological phenomena. Two biological mechanisms are focused on. One is a mTORC1 signaling mechanism which is important to grow cells and the other is a LD reducing mechanism that is related to lipid metabolism. As performing target-based screening, mTORC1 modulators are identified and the LD reducing small molecule is selected by image-based LD monitoring high-contents screening. Using these bioactive small molecules, I desire to approach its mode of action to understand biological phenomena with diverse aspects and suggest new therapeutic strategies to specific disease as an application beyond novel enlightenment.

Chapter 2. A new perspective to modulate mTORC1 through LRS-RagD interaction modulators

2.1. Introduction

mTORC1 responds to amino acids, stress, oxygen, energy, and growth factors [12, 13] and is acutely sensitive to rapamycin. Under nutrient-rich conditions, mTORC1 promotes cell growth and proliferation by stimulating biosynthetic pathways, including mRNA transcription and translation, and by inhibiting cellular catabolism through repression of the autophagy pathway and also drives cell-cycle progression. Thus, we can understand how our body grows through the research about mTORC1 signaling pathway.

Early mTORC1 signaling pathway studies had been understood by Rapamycin. Rapamycin is a natural compound which binds to 12-kDa FK506-binding protein (FPBP12) and disrupts integration of mTORC1 Selective and specific feature of Rapamycin has allowed a variety of mechanism studies on mTORC1 signaling and new mTORC1 inhibitor design [58]. However, recent mTORC1 research field reached the limit because knowledge in mTORC1 pathway related to Rapamycin was saturated and Rapamycin analogs, called Rapalogs, have shown Rapamycin resistance in drug discovery

research [59-62].

As an alternative and novel mode of action to target mTORC1, mTORC1 pathway via amino acid sensing has been focused on [63, 64]. One of the most remarkable mechanism is Leucyl-tRNA synthetase (LRS) and Ras-like GTPase D (RagD) interaction [30]. LRS has a canonical role to catalyze the conjugation of leucine (Leu) to its cognate tRNA to form an aminoacyl-tRNA, which serves as a precursor for protein synthesis. In 2012, Kim's group reported that a noncanonical role of LRS in amino acid-dependent mTORC1 activation. According to this study, LRS can sense and charge Leu to activate mTORC1 and binds to RagD-GTP protein to form a LRS–RagD protein complex in a Leu-dependent manner, which leads to translocate mTORC1 to the lysosome membrane and subsequent activation of mTORC1. Thus, LRS–RagD interaction could serve as a Leu-sensing mechanism in the amino acid-dependent activation of mTORC1.

The discovery of novel small-molecule PPI modulators of LRS and RagD could shed light on the comprehension of molecular mechanism of mTORC1 activation in an amino acid-dependent manner. In addition, they could serve as lead compounds for the development of potential therapeutic agents with new modes of action to treat human diseases linked to the oncogenic activation of mTORC1 because it has advantages of having less side-effects in the view of targeting not mTORC1 itself but PPI indirectly. Further,

diversification of the 3D molecular shapes of in-house library molecules designed with drug-like core skeletons may lead to various interactions with diverse biopolymers and allow for the identification of specific modulators of challenging targets such as PPIs.

However, LRS-RagD interaction is not good at accessibility as target molecules because the interaction and structures of human LRS and RagD have not yet been fully characterized, therefore, it is impossible to design rationally at hot-spot on the interaction surface. The proper way to identify LRS-RagD modulators is screening of small molecules and I developed ELISA-based high-throughput screening system to discover small molecules modulating LRS-RagD interaction.

2.2. Materials and methods

Antibodies, plasmids and proteins Anti-LC3B (ab51520), anti-S6K1 (ab32359), anti-phsopho-T389 S6K1 (ab2571), and HRP-labeled anti-horse IgG secondary antibodies (ab6802) were purchased from Abcam. Anti-glutathione-S-transferase (GST) antibody (sc-459) was purchased from Santa Cruz Biotechnology. Anti-p62 (CST 5114), anti-glyceraldehyde-3-phosphate dehydrogenase (GAPDH) (CST 2118), anti-phospho-S65 4E-BP1 (CST 9451), anti-phospho-S757 ULK1 (CST 6888), anti-phospho-S473 Akt (CST 4058), anti-

phospho-T172 AMPKα (CST 2531), and HRP-labeled anti-rabbit IgG secondary antibodies (CST 7074) were purchased from Cell Signaling Technology. His-tagged LRS and GST-tagged RagD were in our laboratory stocks. mCherry-GFP-LC3 plasmid (pBabe vector) was from Dr. Heesun Cheong, Division of Chemical Biology, Research Institute, National Cancer Center, Korea.

Instruments and programs To develop ELISA, the absorbance of 96-well plate was measured by BioTek Synergy HT Microplate reader. ChemiDoc^{TM} MP imaging system from Bio-Rad was used for analyzing chemiluminescent signal in western blotting assay. Following signal quantification was done by ImageLab 4.0 program provided by Bio-Rad.

DeltaVision Elite imaging system from GE Healthcare was used for imaging experiment. Objective lenses were equipped with Olympus IX-71 inverted microscope with PLAN APO 60×/Oil (PLAPON60×O), 1.42 NA, WD 0.15 mm. sCMOS camera and InSightSSI fluorescence illumination module were equipped with the system. Four-color fluorescent protein (Live Cell) filter set [GE Healthcare, 52-852113-013] was used for imaging. For live cell imaging, CO_2 supporting chamber with an objective air heater were installed with the system. Images were analyzed with SoftWorks program supported by GE Healthcare. Graphs and figures provided were analyzed with GraphPad Prism 5 program.

Cell Culture HEK293T cell was cultured in Dulbecco modified eagle medium (DMEM) with 10% (v/v) fetal bovine serum (FBS) and 1% (v/v) antibiotic-antimycotic solution. HeLa, DU145, and Ca Ski cell lines were cultured in RPMI 1640 medium with 10% (v/v) FBS and 1% antibiotic-antimycotic solution. Both cells were maintained in 100-mm cell culture dish in an incubator at 37 ℃, in a humidified atmosphere with 5% CO_2.

Leucine Starvation For leucine depletion, cells were rinsed with leucine-free DMEM twice, incubated in leucine-free DMEM for 60 min and replaced with and incubated in DMEM.

ELISA His-tagged human LRS were diluted in carbonate buffer (100 mM, pH 9.6) at the concentration of 0.5 ng/μL. Solution were distributed to the half-bottom 96 well clear plate from CORNING 3690. After incubation overnight at 4 ℃ (sealed), coating solution from each well was removed and washed for three times with phosphate buffered saline with 0.05% Tween® 20 (PBST). 5% bovine serum albumin (BSA) in PBS solution was treated to each well for blocking step, followed by the treatment of each compound and GST-tagged human RagD simultaneously for 3 h. GST protein itself was treated as negative control. Diluted GST antibody in PBST was added and incubated at room temperature for 1 h. After washing with PBST,

the HRP-conjugated anti-horse IgG secondary antibody diluent was treated and incubated at room temperature for 1 h. TMB was added to each well for colorimetric development. Blue color should be developed in positive wells. To stop the color reaction, 1 M H_3PO_4 stopping solution was added. Finally, absorbance at 450 nm were measured.

Western Blotting Cells were lysed with radio-immunoprecipitation assay (RIPA) buffer (50 mM Tris, pH 7.8, 150 mM NaCl, 0.5% deoxycholate, 1% IGEPAL CA-630, protease inhibitor cocktail, and phosphatase inhibitors). Protein was obtained after centrifugation at 15000 rpm for 20 m, by transferring supernatant. Protein concentration was normalized with Micro BCA™ protein assay kit. Overall protein sampling procedure was done at 4 ℃. Prepared protein samples were analyzed with SDS-PAGE and following western blot procedure. Protein was transferred into nitrocellulose membrane after SDS-PAGE experiment. Membrane was blocked with 2% BSA in TBST over 1 h on r. t. Primary antibodies were treated overnight at 4 ℃ [Anti-LC3B (ab51520); 1:1000, anti-S6K1 (ab32359); 1:1000, anti-phsopho-T389 S6K1 (ab2571); 1:800, anti-p62 (CST 5114); 1:1000, anti-glyceraldehyde-3-phosphate dehydrogenase (GAPDH) (CST 2118); 1:1000, anti-phospho-S65 4E-BP1 (CST 9451); 1:1000, anti-phospho-S757 ULK1 (CST 6888); 1:800, anti-phospho-S473 Akt (CST 4058); 1: 1000, anti-phospho-

T172 AMPKα (CST 2531)], followed by washing with TBST. HRP-labeled anti-rabbit IgG secondary antibody (1:5000) was treated at room temperature for 1 h. Antibodies were treated with the concentration indicated in antibody manufacturer's protocol. After washing with TBST, membrane was developed by Amersham ECL prime solution. Chemiluminescent signal was measured by ChemiDoc^{TM} MP imaging system.

Surface Plasmon Resonance (SPR) Assay The dissociation rate constant (KD) toward His-LRS was determined by surface plasmon resonance (SPR) technique at the national center for inter-university research facilities (NCRF) in Seoul National University using a Biacore T100 instrument from GE Healthcare. The carboxyl group on the surface of CM5 sensor chip was replaced with reactive succinimide ester using combination of 1-ethyl-3-(3-dimethylaminopropyl)-carbodiimide (EDC) and N-hydroxysuccinimide (NHS) in flow cells 1 and 2. Human LRS (1.5× PBS, pH 7.3) were immobilized on the flow cell 2 (aimed RU; 12000) through formation of amide bond by reacting with the resulting NHS ester. The remaining NHS ester on flow cells 1 and 2 was quenched by injection of 1 M ethanolamine-HCl (pH 8.0) solution. During the immobilization process, PBS was used as running buffer. After the immobilization of hLRS, compounds were injected for 60 s at a flow rate of 20 μL/min in various concentration from 1 μM to 15 μM. At

the same flow rate, dissociation of compounds from the sensor surface was monitored for 200 s. As a running buffer, 1× PBS (pH 7.3) containing 3% DMSO and 0.005% P20 solution were used. The binding events were measured at 25 ℃. Data analysis were done by using Biacore T100 Evaluation software from GE Healthcare. Final sensorgrams were obtained after the elimination of responses from flow cell 1 and buffer-only control. The dissociation constant (KD) was calculated by fitting the sensorgrams to the 1:1 binding model.

FRET imaging experiment and analysis We carried out FRET imaging with DeltaVision Elite imaging system [GE healthcare]. For maintaining live cell condition during experiment, imaging was performed in a CO_2 supporting chamber along with an objective air heater. HEK293T cells were transfected with LRS-CFP (Condition 1), RagD-YFP (Condition 2) and both LRS-CFP and RagD-YFP (Condition 3). Condition 1 & 2 were for calculating crosstalk and condition 3 was for FRET analysis. Images captured with CFP/CFP, YFP/YFP and CFP/YFP filter sets (excitation/emission) and 60× scale. Excitation filter: 438/24 nm and Emission filter 475/24 nm for CFP; Excitation filter: 513/17 nm and Emission filter: 548/22 nm for YFP. In each experiment, images of randomly selected 4 or 5 different cells per individual condition were taken at 10-min intervals over 3.5 h. Ultimate focusing module was operated before imaging during whole imaging process. Compounds were treated in 30 min after live cell

imaging. Out of focus light is digitally removed using the SoftWorks deconvolution software. FRET analysis controlled by DeltaVision SoftWorks using the SoftWorks tool “FRET analysis” for excluding false-positive signal such as CFP crosstalk and YFP crosstalk. Using ‘FRET analysis’ tool, extract crosstalk information from condition 2 & 3. (CFP crosstalk was extracted from condition 2 on whole time point images and YFP crosstalk was extracted from condition 3 on whole time point images.) Net FRET images were developed by applying each crosstalk extracted from each time point. Calculate FRET efficiency within region of interest of developed Net FRET images. Finally, FRET efficiency was converted to FRET efficiency ratio by level at 30 min as a standard. The quantified data are the mean measurements from 3 independent experiments.

2.3. Results and Discussion

2.3.1. In-house library screening with ELISA-based high-throughput screening system

To identify novel small-molecule PPI modulators of the LRS–RagD interaction, about 4000 in-house small molecule library was subjected to ELISA-based high-throughput screening (HTS) using purified human LRS and GST (glutathione-S-transferase)-tagged RagD where

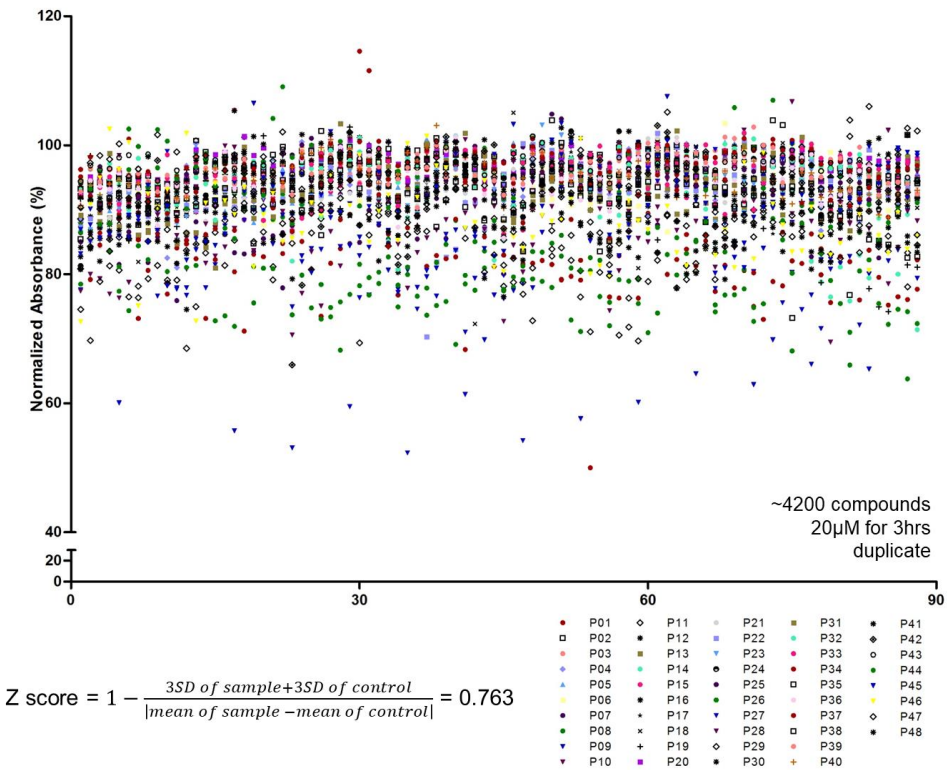

Figure 2.1. ELISA-based screening results. About 4000 in-house library compounds were used to identify LRS-RagD interaction modulators.

the antibody-based signal was lowered or elevated upon treatment with molecules. Screening results are presented on Fig. 2.1. Based on the DMSO control as a normalization standard, over 100% indicates stabilization of LRS-RagD interaction and below 100% means inhibition. From the screening, I was interested in three distinct LRS-RagD modulating compound groups, one stabilizing compound group and two inhibiting compound groups.

2.3.2. Possibility to modulate mTORC1 through LRS-RagD perturbation with small molecules

First, I focused on the stabilizing compounds. The selected LRS–RagD interaction stabilizing were designed as β-turn mimetic compound. The library was synthesized tetra-substituted hexahydro-4H-pyrazino[2,1-c][1,2,4]triazine-4,7(6H)-diones as β-turn mimetic. Through the simple structure and activity relationship analysis, I clearly demonstrated that the hydrophilic core structure with hydrophobic and aromatic substituents stabilized the LRS–RagD interaction more effectively (Fig. 2.2), which is in accordance with its library design rationale, in which hydrophobic substituents on a single β-turn mimetic scaffold enhanced the binding affinity toward the hydrophobic region of hot spots at the PPI interfaces.

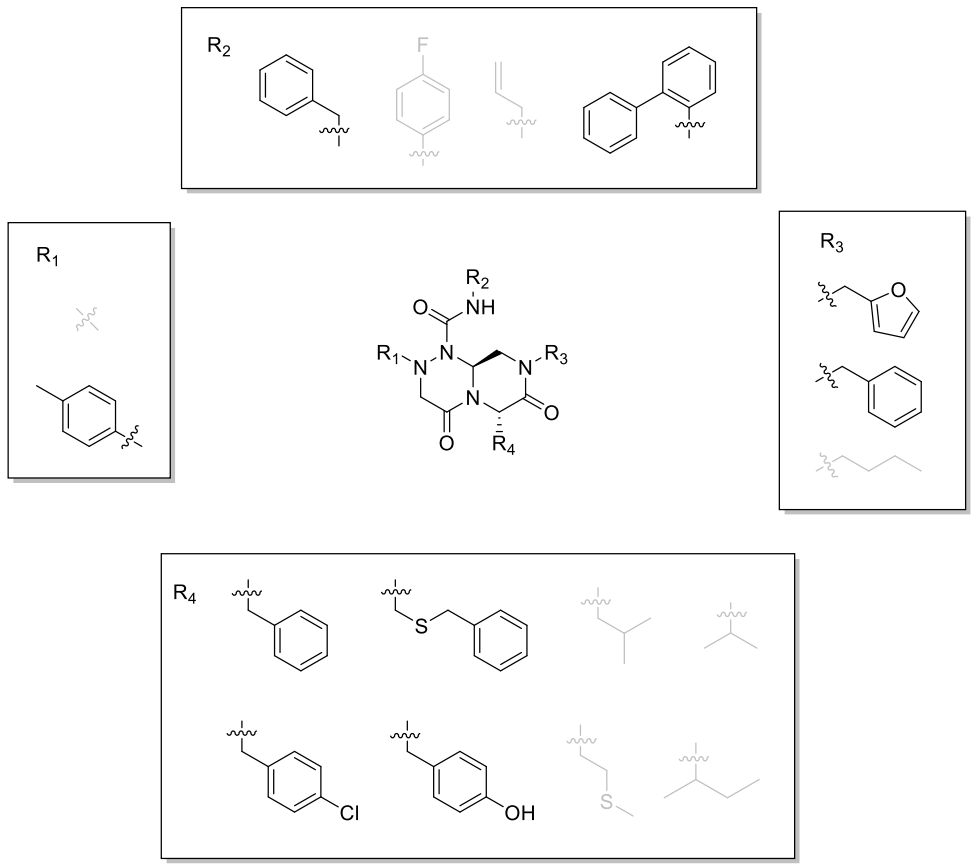

Figure 2.2 Structure and relationship pattern. Compounds which have aromatic rings in the structure might have better stabilizing activities between LRS and RagD interaction.

After selecting a series of hit compounds from the screening, western blot analysis of T389 phosphorylated p70 ribosomal protein S6 kinase 1 (S6K1), one of the typical mTORC1 substrates, was performed to determine whether these compounds could affect the activity of mTORC1 by stabilizing the LRS–RagD interaction. As shown in Fig. 2.3, the presence of leucine can initiate the LRS and RagD interaction, which is essential for the activation of mTORC1 and phosphorylation of the subsequent S6K1. Under leucine deprived

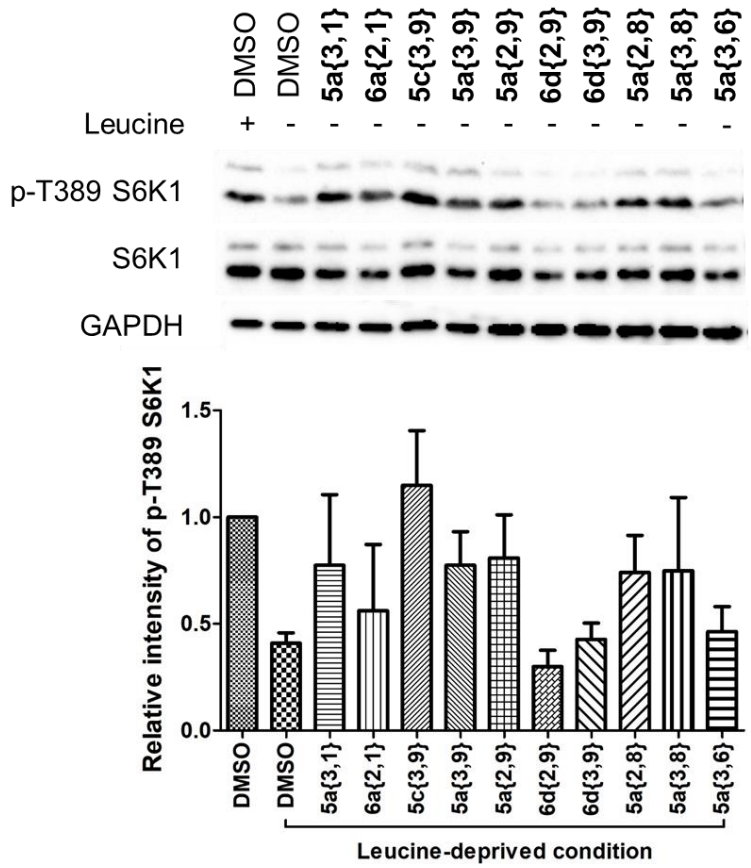

Figure 2.3. Hit compound selection. HEK293T cells were starved for leucine for 1 hour and treated with 20 μM compounds for 3 hours in leucine-free condition. Phospho-T389 S6K, S6K and GAPDH were determined by western blotting analysis. HEK293T cells treated with 0.6 mM leucine were used as controls.

conditions, phosphorylated S6K1 decreased because of the inactivation of mTORC1. However, the phosphorylation level of S6K1 was successfully restored upon treatment with our b-turn mimetic compounds, as the LRS–RagD PPI conferred stability even under leucine-deprived conditions. Among the initial hit compounds, I identified the most potent compound based on the relative intensity of phosphorylated S6K1 in the Leu-deprived media compared to that in

normal media and selected **5c{3.9}** for further biophysical analysis [65].

Using ELISA and western blot analysis, I confirmed that **5c{3,9}** stabilized the in vitro interaction between LRS and RagD and regulated the activity of mTORC1, leading to the restoration of phosphorylated S6K1 levels under leucine-deprived conditions (Fig. 2.4A and B). However, this observation was not enough to confirm the stabilization of the direct LRS–RagD interaction. To confirm this, a novel biophysical assay using fluorescence resonance energy transfer (FRET) was established to examine the interaction between CFP (Cyan Fluorescent Protein)-fused LRS (LRS-CFP) and YFP (Yellow Fluorescent Protein)-fused RagD (RagD-YFP) in live cells: the extent of the LRS and RagD direct interaction was measured as the intensity of the FRET signal between CFP and YFP (Fig. 2.4C). To precisely quantify the FRET efficiency, some single cells were selected to track over time and live cell imaging was conducted at CFP/CFP, CFP/YFP, and YFP/YFP filter sets. Finally, the captured images were analyzed to exclude false-positive signals such as CFP and YFP crosstalk. As shown in Fig. 2.4D and E, I observed that the FRET efficiency between CFP and YFP was increased over time upon treatment with **5c{3,9}**, confirming the **5c{3,9}**-mediated stabilization of the LRS and RagD interaction under live cell conditions. For the less potent compound **5a{2,9}**, I observed marginal changes in the FRET efficiency that were similar to those in the DMSO control. This FRET-

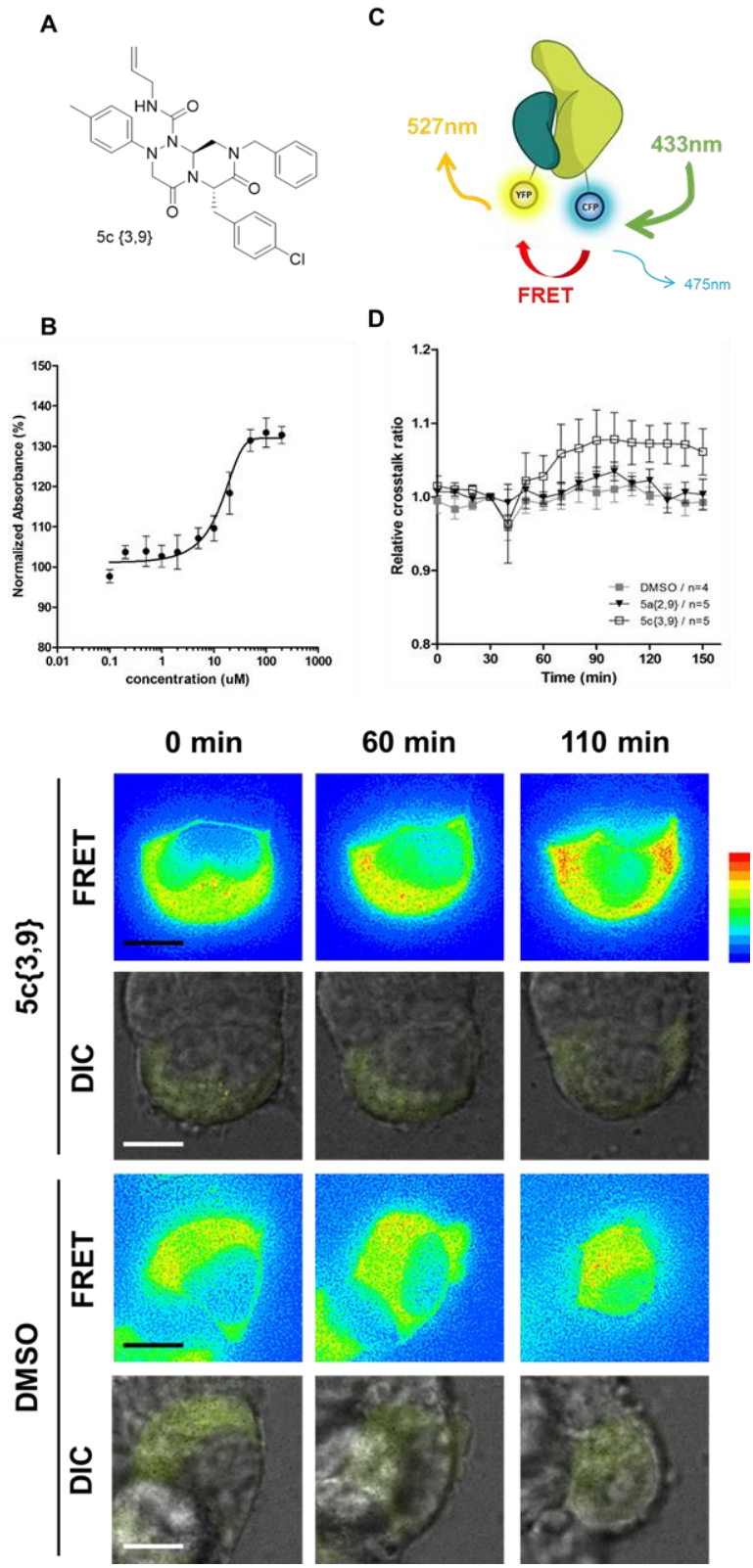
A
5c {3,9}
C
527nm
433nm
YFP
CFP
FRET
475nm
B
Normalized Absorbance (%)
concentration (uM)
D
Relative crosstalk ratio
Time (min)
DMSO / n=4
5a{2,9} / n=5
5c{3,9} / n=5
0 min
60 min
110 min
5c{3,9}
FRET
DIC
DMSO
FRET
DIC

based biophysical experiment supported that **5c {3,9}** stabilized LRS–RagD interaction directly in the cellular system and modulated the activity of mTORC1.

It is difficult to identify small-molecule modulators of specific PPIs, but it is even more difficult to identify PPI stabilizers from a small molecule library [66]. Though some limitations, the compounds were identified LRS-RagD modulators for the first time and showed the possibility to regulate mTORC1 with the PPI perturbation.

Figure 2.4. Confirmation of protein-protein interaction modulation in cellular system. (A) Hit compound, **5c{3,9}**, structure. (B) **5c{3,9}** showed stabilizing activity between LRS-RagD interaction in a dose-dependent manner. (C) Schematic representations of FRET phenomenon between CFP-LRS and YFP-RagD. When LRS interacts with RagD, CFP bound LRS approaches to YFP bound RagD, which causes FRET, fluorescence of 475 nm from CFP with excitation at 433 nm transfer to YFP fluorescence of 527 nm. (D) Representative calculated FRET within a 293T cells co-expressing LRS-CFP and RagD-YFP. Cells were co-transfected with LRS-CFP and RagD-YFP and treated **5c{3,9}** 40 μM or DMSO. Images were taken at 10-min intervals over 2.5 hours in live cell condition. The color scale indicates the range of FRET intensity, from low (blue) to high (red). Scale bar, 20 μm. (E) Relative crosstalk ratio over time were calculated from each time point images. Compound were treated after 40 m from imaging start point.

2.3.3. Distinct perturbation of mTORC1 by LRS-RagD inhibition

Through LRS-RagD stabilization study, I confirmed mTORC1 perturbation via LRS-RagD is possible. With a parallel project to **5c{3,9}**, LRS-RagD inhibitors were also identified. The screening exercise led to the identification of aziridine containing **20f** and **21f** as dose-dependent inhibitors of the LRS–RagD interaction (Fig. 2.5A and B) [67].

On the basis of the previous study, I hypothesized that **20f** and **21f** might inhibit the LRS-mediated Leu signaling to mTORC1 via direct disruption of the LRS–RagD interaction. As shown in Fig. 2.5C, the level of phosphorylated T389 S6K1 was suppressed upon **20f** and **21f** treatment even in the presence of Leu. On the basis of the reduction of LRS–RagD interaction by ELISA (**20f** 15.5%; **21f**30.2%) and the suppression of phosphorylated S6K1 by western blotting (**20f** 16.4%; **21f** 48.9%), **21f** was selected as the potent inhibitory compound and subjected it to further western blot analysis and biophysical study using surface plasmon resonance (SPR) spectroscopy.

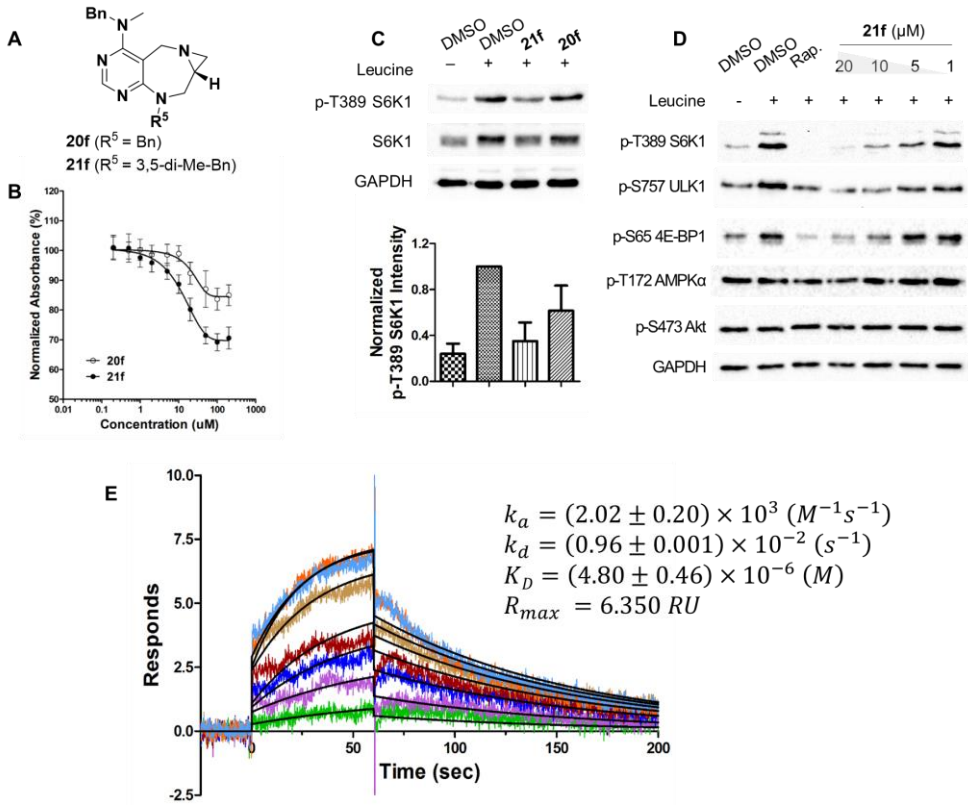

Figure 2.5. Discovery of chemical modulator for LRS–RagD interaction. (A) structure of **20f** and **21f**. (B) Dose–response curves in ELISA of **20f** and **21f**. The results represent the mean of three biological replicates; error bars represent the s.e.m. (C) Effects of **20f** and **21f** on mTORC1 signaling pathway. HEK293T cells were treated with 20 μM of **20f** and **21f** for 3 h. As a negative control, cells were deprived of leucine for 3 h. Level of phospho-T389 S6K1 were quantified against a DMSO control. The bar graph represents the mean of five biological replicates; error bars represent the s.e.m. (D) Dose-dependent effects of **21f** to mTORC1 signaling pathway. HEK293T cells were treated with 20, 10, 5 and 1 μM of **21f** for 3 h. As a negative control, cells were deprived of leucine for 3 h. Rapamycin (Rap) was used as a positive control and cells were treated with 200 nM of Rap for 3 h. (e) Sensorgrams of SPR spectroscopy of **21f** showed its concentration-dependent binding to purified LRS. The concentration plotted are 1, 2.5, 5, 10, 12.5, 15, 17.5 and 20 μM, in order of increasing **21f**. The curve fittings are shown in black. The sensorgrams represent the mean of two biological replicates.

As shown in Fig. 2.5D and Fig. 2.6A, **21f** downregulated not only the phosphorylation of S6K1 but also eukaryotic translation initiation factor 4E-binding protein 1 (4E-BP1) S65 phosphorylation [68] and mammalian autophagy-initiating kinase (ULK1) S757 phosphorylation [69], known substrates of mTORC1 kinase, in a dose-dependent manner in HEK293T cell lines and two additional cell lines, Ca Ski cervical cancer cell and DU145 prostate cancer cell lines. Interestingly, **21f** affected neither mTORC2 signaling pathway (the level of phospho-S473 Akt), nor the energy-dependent AMP-activated protein kinase (AMPK) signaling pathway (the level of phospho-T172 AMPKα) (Fig. 2.5D and Fig. 2.6A). This observation confirmed the selective inhibitory activity of **21f** toward mTORC1 signaling pathway over mTORC2 or other energy mediated signaling pathway. In addition, **21f** inhibited the phosphorylation of mTORC1 substrates over 12 h (Fig. 2.6A), which is similar to Rapamycin (Rap), one of the classic selective mTORC1 inhibitors (Fig. 2.6B). However, the general inhibitory pattern of **21f** on mTORC1 pathway was quite different from that of Rap, particularly the phosphorylated S757 ULK1, which provides the clue that **21f** has a different mode of action from that of Rap via specific inhibition of LRS–RagD interaction. At the same time, the gradual loss of **21f**'s activity might be caused by the negative feedback loops in the mTORC1 signaling pathway or metabolic clearance of **21f** in the cellular system.

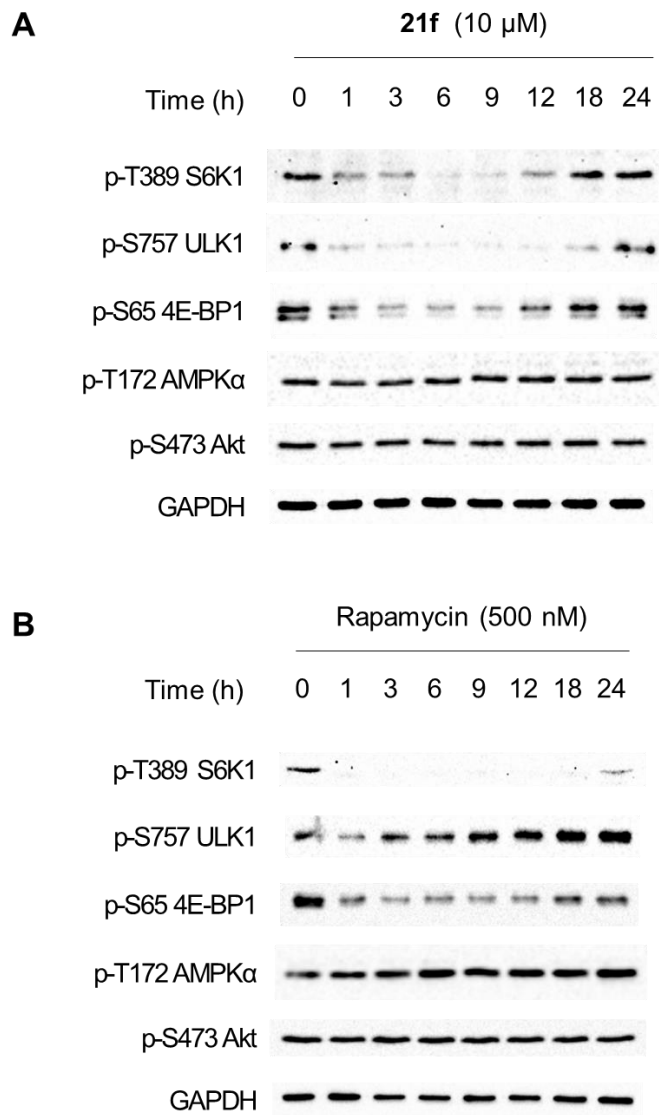

Figure 2.6. Time-course study of the inhibitory effect of **21f** and Rapamycin on mTORC1 signaling pathway for 0–24 h. (A) HEK293T cells were treated with 10 μM of **21f**. (B) HEK293T cells were treated with 500 nM Rapamycin for specified time in complete media. Phospho-T389 S6K1, phospho-S757 ULK1, phospho-S65 4E-BP1, phospho-T172 AMPKα, phospho-S473 Akt, S6K1 and GAPDH were determined by western blot. The western blot results shown are representative of three biological replicates.

The subsequent biophysical study using SPR revealed the binding affinity patterns of **21f** and other pyrimidodiazepine-containing scaffolds (**14f** and **19f**) towards purified LRS. I clearly observed the 1:1 binding event in the SPR sensorgrams of **21f** with KD value of 4.8 (±0.46) μM and the saturation event at the high dosage (Fig. 2.5E), whereas **14f** and **19f** showed no dose-dependent responses without any specific binding events, which supported that **21f** specifically binds LRS and disrupts the interaction between LRS and RagD.

2.3.4. Different effects on mTORC1 of serum and LRS-RagD interaction

In the case of **21f**, it showed quite cytotoxicity not to be proper for the further study. Instead of **21f**, another LRS-RagD interaction inhibitory compounds group was preferable owing to less cytotoxicity and interesting structure and activity relationship. As shown in Fig. 2.1, some compounds from the same library exhibited PPI inhibition pattern periodically which means the active compounds are sharing the same substituents. This library was also designed as β-turn mimicking compounds bearing oxopiperazine as privileged structure and only tetra-substituted oxopiperazine-based structure with methyl-piperazine moiety in R_3 position actually showed LRS-RagD inhibition activity (Fig. 2.7).

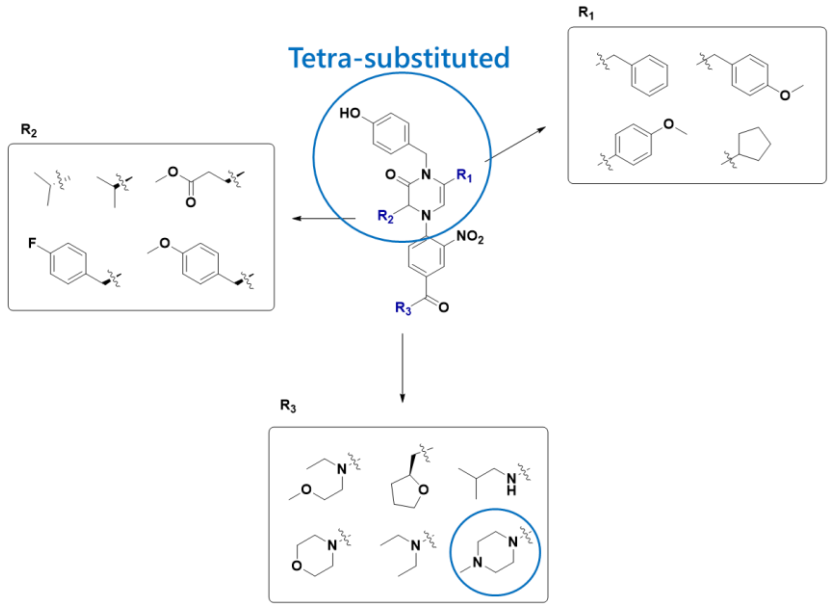

Figure 2.7. Structure and relationship pattern. Tetra-substituted oxopiperazine-based structure with methyl-piperazine moiety in R_3 position actually showed LRS-RagD inhibition activity

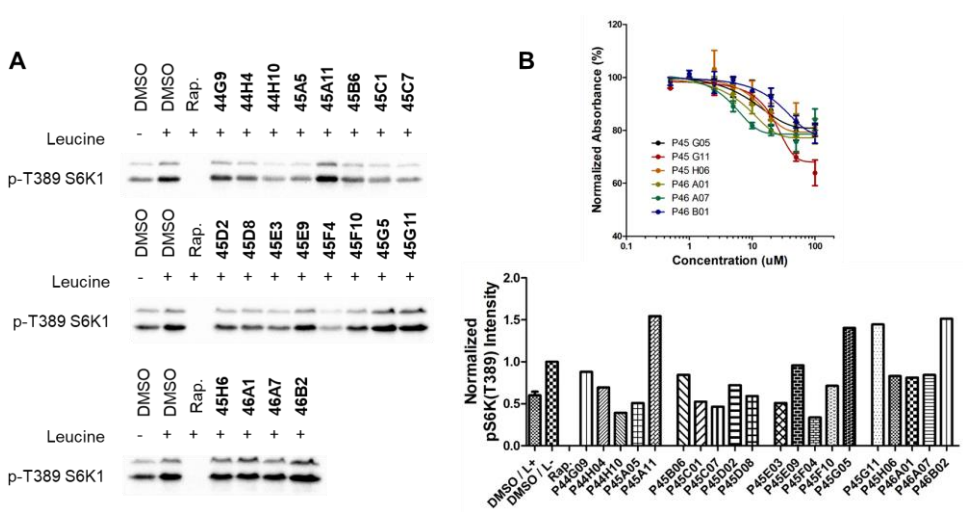

Figure 2.8. Hit selection

Over the series compounds, **P45F04** was selected through phosphorylated T389 S6K1 inhibitory effects in western blotting analysis (Fig. 2.8 and Fig. 2.9A and B). **P45F04** inhibited LRS-RagD interaction dose dependently in ELISA system. To confirm whether this compound suppressed mTORC1 activity in cellular system, western blotting analysis to phosphorylation of mTORC1 substrates, S6K1, 4E-BP1 and ULK1 was conducted. **P45F04** blocked phosphorylation of three mTORC1 substrates in dose dependent manner (Fig. 2. 9C). Additional remarkable aspects were that **P45F04** did not affect to mTORC2 pathway or AMPKα pathway. On time course study, the compound maintained mTORC1 inhibitory activity over 12 hours without perturbation on mTORC2 or AMPKα pathway (Fig. 2.9D). This inhibition pattern was different from that of **21f** (Fig. 2.6A) or Rapamycin (Fig. 2.6B) and similar to that in leucine deprivation condition (Fig. 2.9E).

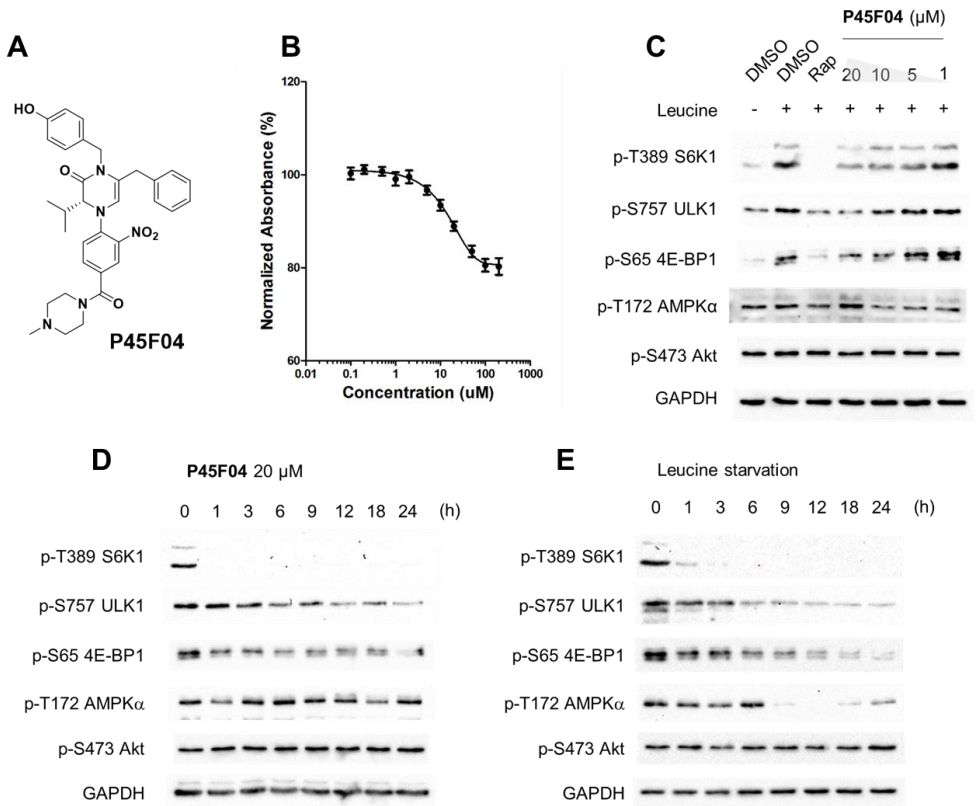

Figure 2.9. Activity Evaluation of **P45F04** (A) Hit compound structure. (B) Dose-response curves in ELISA. **P45F04** inhibits LRS and RagD interaction. (C) 293T cells were treated with 20, 10, 5, 1 μM **P45F04** or 200 nM Rapamycin for 3 h in complete condition. For negative control, 293T cells were starved for leucine for 3 hr. P-S757 ULK1, p-S65 4E-BP1, p-T389 S6K1, GAPDH, p-S473 Akt and p-T172 AMPKα were determined by western blot. (D) 293T cells were treated with 20 μM of **P45F04** for various time in complete media. (E) 293T cells were starved with leucine for various time. P-S757 ULK1, p-S65 4E-BP1, p-T389 S6K1, GAPDH, p-S473 Akt and p-T172 AMPKα were determined by western blot.

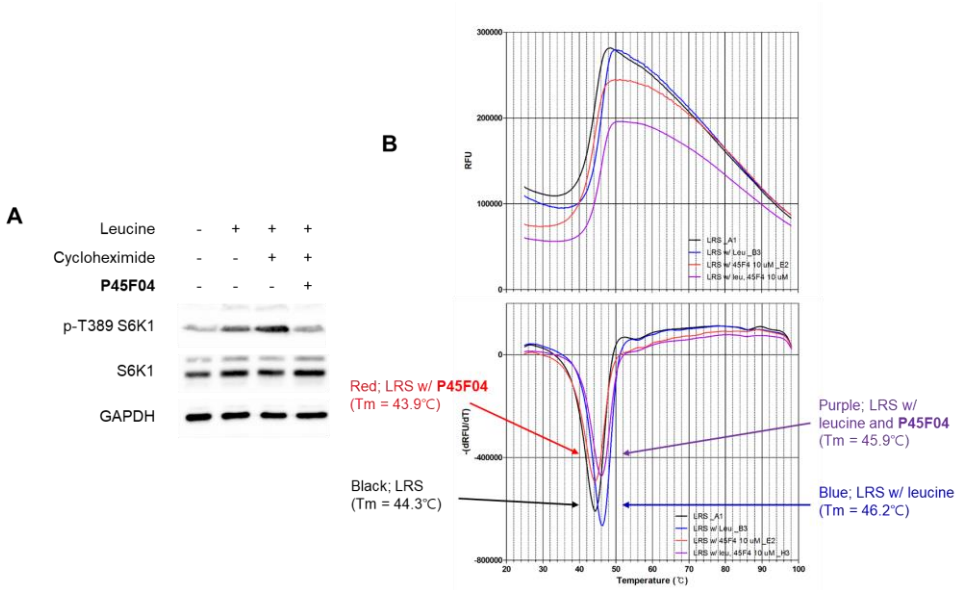

Figure 2.10. Leucine sensing signaling. (A) 293T cells treated with **P45F04** 20 μM and/or Cycloheximide 200 ng/ml. Leucine-free condition were used as controls. p-T389 S6K1, S6K1 and GAPDH were determined by western blot. (B) Differential scanning fluorimetry of LRS. Thermal denaturation curves obtained for LRS with or without leucine (45 μM) and **P45F04** (10 μM).

To specify a binding mechanism of **P45F04**, first, I checked **P45F04** affected on leucine signaling or leucine sensing itself (Fig. 2.10A). Cycloheximide is a protein synthesis inhibitor and it makes cellular amino acid concentration high to activate mTORC1. Phosphorylation of S6K1 increased upon Cycloheximide treatment but in the case of **P45F04**, phosphorylated S6K1 decreased like a basal level. Therefore, I demonstrated it affected leucine sensing signaling. Next, differential scanning fluorimetry (DSF) was carried out (Fig. 2. 10B). The assay principle is based on the thermal stabilization of the native protein structure upon the ligand binding. By measuring fluorescence with gradual temperature increase,

protein (with ligand) melting temperature was determined. LRS's melting temperature was measured about 44℃ and leucine binding LRS denatured about 46℃. In **P45F04** existence with LRS, melting temperature was similar to LRS itself and LRS with leucine and **P45F04** had the same melting temperature to LRS with leucine. From the results, I verified **P45F04** did not disturb leucine sensing itself. Third, FRET imaging between LRS and RagD in live cell was conducted to demonstrate **P45F04** inhibits PPI. Cells overexpressing CFP fused LRS and YFP fused RagD by transfecting plasmid were treated with compound after 30 minutes from starting imaging. After imaging, FRET signals converted to FRET efficiency using software to exclude false-positive signals such as CFP crosstalk and YFP crosstalk. Calculated FRET efficiency were represented as heat map (Fig. 2.11). Instead DMSO and Rapamycin maintained FRET efficiency over time after compound treatment, cells treated with **P45F04** lost FRET signal over time. The results proved that **P45F04** inhibited LRS-RagD interaction.

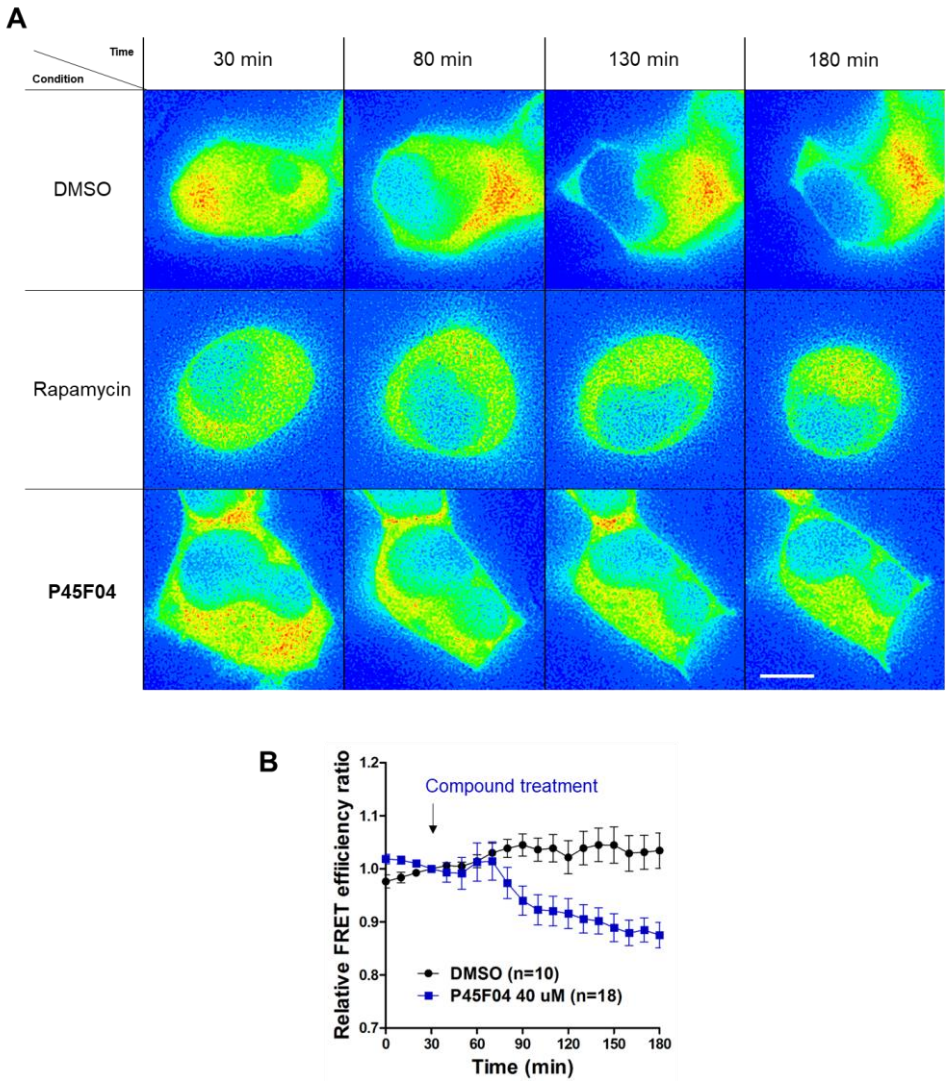

Figure 2.11. Time-lapse FRET imaging between LRS and RagD in live cell condition. (A) Representative calculated FRET images within a 293T cells. Images were taken at 10-min intervals over 3 h in a single cell. **P45F04** (black circle) was treated at 40 μM concentration in 30 min after live cell imaging. (B) Relative FRET efficiency ratio over time were calculated from images with CFP/CFP, CFP/YFP, YFP/YFP filters (excitation/emission) at each time point. Captured FRET images were analyzed using imaging software for excluding false-positive signal such as CFP crosstalk and YFP crosstalk. Scale bar, 7.5 μm.

2.3.5. Sensitizing effects to anti-cancer drug

One interesting point is that **P45F04** affected to mTORC1 much better in serum-free condition than in normal condition (Fig. 2.12), which demonstrated that LRS-RagD interaction signaling is orthogonal to growth factor-mediated mTORC1 activation pathway. Although serum deprivation effects were more powerful than LRS-RagD inhibition, **P45F04** inhibited mTORC1 activity partially and constantly even in fully serum acceptable condition, which is similar to that in leucine deprived condition (Fig. 2.12). Even if **P45F04** did not show very powerful mTORC1 inhibition effects, it would be a more proper cancer treatment strategy because 1) it could lessen side-effect on cell growth and proliferation, 2) it could give selectivity to cancer cells using more amino acids than normal cells and 3) combination therapy

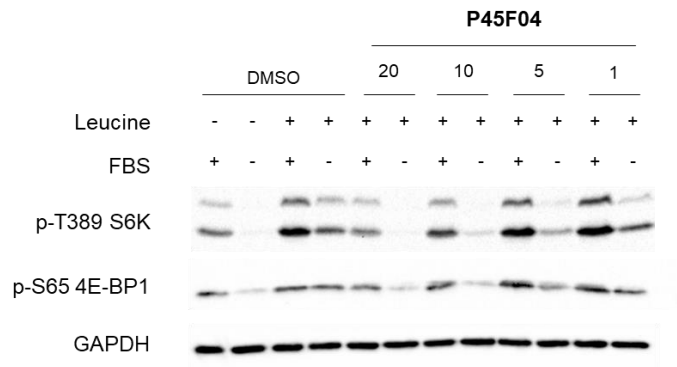

Figure 2.12. **P45F04** activity on serum free condition. 293T cells were treated with 20, 10, 5, 1 μM of **P45F04** for 3 h in complete media or serum-free media condition. For negative control, 293T cells were starved for leucine for 3 h. Phospho-T389 S6K, p-S65 4E-BP1 and GAPDH were determined by immunoblotting.

have been taken center stage to treat cancers [70].

To determine IC_{50} on cell viability and proliferation, MTT assay was carried out (Fig. 2.13). Cervical cancer cell line, HeLa, colorectal cancer cell line, HCT116, breast cancer cell line, MDA-MB-231 and kidney cancer cell line, Caki-1 cells were tested dose dependent cytotoxicity over time. Broadly speaking, IC_{50} at 24 h was about 30 μM and at 48 h and 72 h, IC_{50} was about 20 μM. These results implied that the compound is not cytotoxic but it affected cells steadily over time and blocked leucine sensing mechanism for cell proliferation.

Because its cytostatic but steady leucine sensing blocking effects, I hypothesized that it could act a sensitizer of general anti-cancer drugs. Generally, anti-cancer drugs have severe side effects, cytotoxicity because of lack of selectivity. Therefore, it is necessary to reduce drug's dose as low as possible. In this regard, **P45F04** would be expected to influence on cancer cell more powerful because cancer cells try to take advantage of amino acids exclusively. With like this strategy, cells were treated with general anticancer drug, Taxol and **P45F04** simultaneously and monitored cytotoxicity over time (Fig. 2. 14). As a results, Caki-1 and HeLa cell line showed synergetic cytotoxic effects from which I confirmed **P45F04** could be used as a sensitizer to anti-cancer drugs.

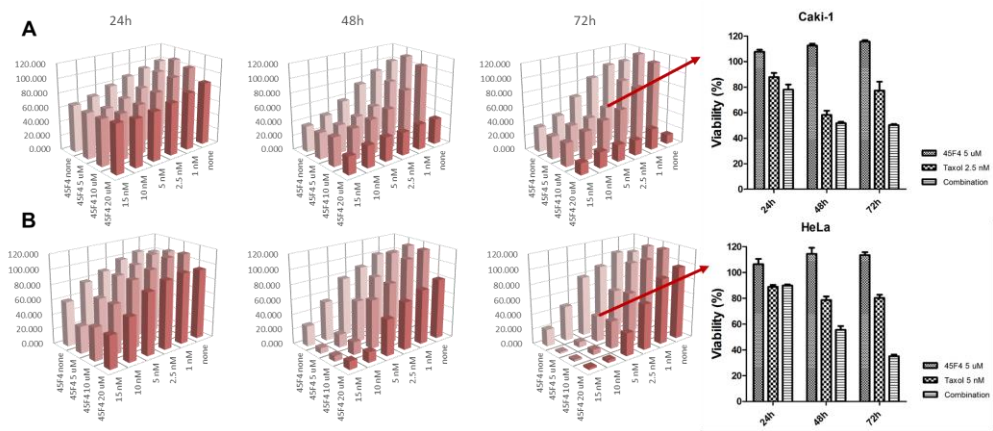

Figure 2.13. Cell viability and proliferation assay on various cell lines upon treatment of **P45F04**

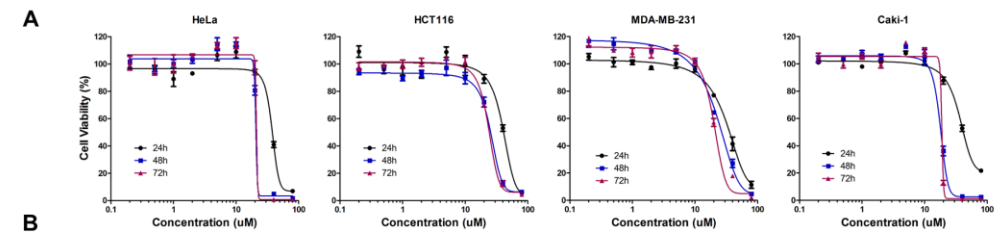

IC50 (μM)	HeLa	HCT116	MDA-MB-231	Caki-1
24h	37.51	39.75	28.89	35.66
48h	20.71	25.42	18.63	17.80
72h	21.18	23.41	19.59	18.88

Figure 2.14. Anti-cancer drug sensitizing effects. (A) Caki-1 and (B) HeLa cells were treated with **P45F04** and/or Taxol for 24, 48 and 72h. Cell Viability was measured by MTT assay

2.4. Conclusion

Nutrient sensing, particularly amino acid sensing, is extremely important for cell survival, but there are no effective methods for dissecting the amino acid-mediated activation of mTORC1. Leucine is an essential amino acid in cells and plays a vital role in modulating mTORC1 activity. Therefore, the discovery of novel small-molecule PPI modulators of LRS and RagD could shed light on the comprehension of a novel molecular mechanism of mTORC1 activation in an amino acid-dependent manner and used to reveal the non-canonical role of LRS.

To identify novel small-molecule PPI modulators of the LRS–RagD interaction, about 4000 in-house small molecule library was subjected to ELISA-based high-throughput screening (HTS). From the screening, three distinct LRS-RagD modulating compound groups, one stabilizing compound group and two inhibiting compound groups, were selected for further study.

β-turn mimetic bicyclic compound **5c{3,9}** selectively activated mTORC1, a key protein complex of cell growth and proliferation, with a novel mode of action—direct stabilization of the LRS–RagD interaction which was verified with time-lapse FRET imaging in live cell condition between LRS-CFP and RagD-YFP. **5c{3,9}** maintained the cells under normal conditions even in the leucine-deprived media. It was the first report to targeting LRS-RagD selectively with a small

molecule and I demonstrated LRS-RagD modulation is a possible way to perturb mTORC1 activity.

To understand mTORC1 signaling pathway via LRS-RagD interaction in terms of a therapeutic target, some active small molecules were selected. Among them, **21f** selectively inhibited mTORC1 activity even in the presence of Leu by binding to LRS and disrupting the LRS–RagD interaction. As **21f** as a LRS binder, it showed distinct inhibitory pattern from Rapamycin and regulated mTORC1 separated from growth factor mediated or energy mediated signaling pathway, which infers that LRS-RagD interaction might be orthogonal to other mTORC1 regulating signaling pathway.

Further, another LRS-RagD interaction inhibitory compound, **P45F04**, was preferable owing to less cytotoxicity and interesting structure and activity relationship study. **P45F04** also inhibited mTORC1 by inhibiting LRS-RagD interaction but it is different from **21f** regarding binding mode. **P45F04** inhibited PPI instead of LRS binding or leucine sensing. Although mTORC1 inhibitory effects through LRS-RagD inhibition by **P45F04** was overwhelmed by growth factor-mediated signaling pathway, its partial but constant mTORC1 inhibition activity would be a more proper cancer treatment strategy because 1) it could lessen side-effect on cell growth and proliferation, 2) it could give selectivity to cancer cells using more amino acids than normal cells and 3) combination therapy have been taken center stage to treat cancers. As a results, I confirmed that

P45F04 sensitized anti-cancer drug effects.

A series of studies would be a great helpful tool compound to challenging PPI research fields and mTORC1 signaling pathway research and also it could be used to therapeutic candidates having a novel mode of action, LRS-RagD interaction modulation.

Chapter 3. Discovery of a novel mechanism of lipid droplet reduction by lipophagy-inducing compound

3.1. Introduction

Lipid droplet (called LD) is a specialized organelle used for cellular free fatty acid storage as a neutral lipid form such as triacylglycerol or sterol esters. Neutral lipids are surrounded with phospholipids and some surface proteins such as perillipin families and lipases [40]. This well-shaped organelle can make itself store lipid efficient manner and avoid lipotoxicity of free fatty acid [36, 38].

LD is very dynamic organelle which can change its forms over their environment such as tissue types and energy conditions [39]. When adipose cells absorb too much fats, LD stores free fatty acid as much as possible and make itself big. The other way, in starved condition, stored lipids may be used for membrane components and energy sources needed and the number and size of LD are reduced. Therefore, LD plays an important role in energy homeostasis and lipid metabolisms [71].

Since LD comes out into the open, many biological mechanisms are identified, however, more specific studies are necessary because the basic LD regulating mechanisms have not even defined in details.

Furthermore, LD research field have been emerged as a major interest because of its importance in biological and physiological systems in both academic and industrial field though its limited information and research pools. The relationship between LD and metabolic diseases has been closed each other. Accumulation of LD in muscle, liver tissue goes as far as to be considered as a hallmark of metabolic diseases such as type 2 diabetes, obesity and atherosclerosis [56, 57].

Therefore, the discovery of bioactive small molecule modulating LD is quite interesting views to study about LD from a chemical biology perspective. Monitoring LD enables us to access metabolic status and metabolic disease related mechanisms because LD itself is regarded as a good phonotype representing cellular metabolic states. Phonotype-based screening is suitable for the discovery because it is not restrained the limited information like LD research and it is possible to approach unbiased and varied manner, which allows opportunities to identify novel LD modulation mechanisms.

In this chapter, study about a novel LD reduction mechanism which is engaged in mode of action of bioactive small molecule is described. To identify a bioactive small molecule, image-based LD monitoring high-contents screening system was used in live cell. The molecule discovered from phenotype-based screening, with LD as a phonotype, activates LD’s clearance mechanism via autophagy process, lipophagy. From the compound, a novel LD reduction mechanisms are investigated and, finally, this study suggests non-

alcoholic steatohepatitis (NASH) treatment strategy through the investigated mechanism.

3.2. Materials and methods

Antibodies and plasmids Anti-LC3B (ab51520), anti-ubiquitin for immunofluorescence (ab7780), anti-ubiquitin for western blotting (ab134953) were purchased from Abcam. Anti-p62 antibody with mouse IgG (sc-28350) was purchased from Santa Cruz Biotechnology. Anti-ATF4 (CST 11815), anti-CHOP (CST 2895), anti-p62 with rabbit IgG (CST 5114), anti-glyceraldehyde-3-phosphate dehydrogenase (GAPDH) (CST 2118) HRP-labeled anti-mouse IgG (CST 7076) and HRP-labeled anti-rabbit IgG secondary antibodies (CST 7074) were purchased from Cell Signaling Technology. mCherry-GFP-LC3 plasmid (pBabe vector) was from Dr. Heesun Cheong, Division of Chemical Biology, Research Institute, National Cancer Center, Korea. mCherry-LC3 plasmid was purchased from Addgene (40827).

Instruments and programs ChemiDoc™ MP imaging system from Bio-Rad was used for analyzing chemiluminescent signal in western blotting assay. Following signal quantification was done by ImageLab 4.0 program provided by Bio-Rad.

DeltaVision Elite imaging system from GE Healthcare was used

for imaging experiment. Objective lenses were equipped with Olympus IX-71 inverted microscope with PLAN APO 60×/Oil (PLAPON60×O), 1.42 NA, WD 0.15 mm. sCMOS camera and InSightSSI fluorescence illumination module were equipped with the system. Four-color fluorescent protein (Live Cell) filter set [GE Healthcare, 52-852113-013] was used for imaging. For live cell imaging, CO_2 supporting chamber with an objective air heater were installed with the system. Images were analyzed with SoftWorks program supported by GE Healthcare. Graphs and figures provided were analyzed with GraphPad Prism 5 program.

Cell Culture Hep G2 cell was cultured in Dulbecco modified eagle medium (DMEM) with 10% (v/v) fetal bovine serum (FBS) and 1% (v/v) antibiotic-antimycotic solution. HeLa cell was cultured in RPMI 1640 medium with 10% (v/v) FBS and 1% antibiotic-antimycotic solution. Both cells were maintained in 100-mm cell culture dish in an incubator at 37 ℃, in a humidified atmosphere with 5% CO_2.

LD screening For the image-based screening in a high-throughput manner, HeLa cells were seeded on a 96-well black plate with clear bottom. Using 96 solid pin multi-blot replicators, various compounds from in-house chemical library were transferred to individual wells of a 96 well plate with their final concentration as 10

μM. Individual screening plates contained oleic acid as a positive control, serum-free condition as a negative control, and DMSO as a vehicle. After 24 h incubation at 37 ℃, SF44 (5 μM) and Hoechst 33342 (2 μg/ml) were added to cells charged in individual wells. Serum-free condition (negative control) was needed to exchange its media with regular media before the treatment of SF44 and Hoechst. After 30 m incubation, automatic fluorescence imaging of designated plates was performed with InCell Analyzer 2000 (GE Healthcare) without any washing steps. Images of randomly selected 4 different spots per individual well in a 96-well plate were automatically captured. Images were taken by auto-focusing mode and 20× scale. Fluorescence imaging was performed at the indicated filter setting; Excitation filter: 430/24 nm and Emission filter 605/64 nm for LD; Excitation filter: 350/50 nm and Emission filter: 455/50 nm for nuclei. Data were analyzed by InCell Developer program according to the manufacturer's protocol. Fluorescence intensity of LD was interpreted as a cellular organelle using granularity module and the area of individual cell was recognized by nuclei staining using collar segmentation.

Western Blotting Cells were lysed with radio-immunoprecipitation assay (RIPA) buffer (50 mM Tris, pH 7.8, 150 mM NaCl, 0.5% deoxycholate, 1% IGEPAL CA-630) with deubiquitinating enzymes inhibitors (10 mM N-Ethylmaleimide, 5

mM EDTA), phosphatase inhibitors (5 mM NaF, 2 mM Na_3VO_4) and protease inhibitor cocktail (Roche). Proteins were obtained after centrifugation at 15000 rpm for 20 m, by transferring supernatant. Protein concentration was quantified with Micro BCA™ protein assay kit. Overall protein sampling procedures were done at 4 ℃. Prepared protein samples were analyzed with SDS-PAGE and following western blot procedure. Proteins were transferred into nitrocellulose membrane and it was blocked with 2% BSA in TBST over 1 h on r. t. Primary antibodies were treated overnight at 4 ℃ [Anti-LC3B (ab51520); 1:2000, anti-p62 with rabbit IgG (CST 5114); 1:1000, anti-glyceraldehyde-3-phosphate dehydrogenase (GAPDH) (CST 2118); 1:2000, anti-ubiquitin (ab134953); 1:1000, anti-p62 with mouse IgG (sc-28350); 1:100, anti-ATF4 (CST 11815); 1:1000, anti-CHOP (CST 2895); 1:1000], followed by washing with TBST. HRP-labeled anti-rabbit IgG secondary antibody or HRP-labeled anti-mouse IgG secondary antibody (1:5000) were treated at r. t. for 1 h. After washing with TBST, membrane was developed by Amersham ECL prime solution. Chemiluminescent signal was measured by ChemiDoc™ MP imaging system.

Transfection HeLa cells were seeded on Lab-Tek II Chambered Coverglass w/Cover #1.5 Borosilicate Sterile/8 Well (Nunc 155409), 24 h before transfection. mCherry-GFP-LC3 plasmid or mCherry-hLC3 plasmid was transfected to HeLa cell using Lipofectamine 2000

reagent. Transfection was proceeded according to manufacturer's protocol.

mCherry-GFP-LC3 puncta imaging DeltaVision Elite imaging system was used for the imaging of mCherry-GFP-LC3 transfected HeLa cell. For live-cell imaging, chamber was maintained at 37 ℃, 5% CO_2 condition. Image was obtained with 60× scale, using mCherry/mCherry, GFP/GFP (Excitation/Emission) filter sets. mCherry (excitation: 575/25 nm, emission: 625/45 nm); and GFP (excitation: 475/28 nm, emission: 525/48 nm). Images were analyzed with SoftWorks deconvolution software.

mCherry-hLC3 and LD imaging DeltaVision Elite imaging system was used for the imaging of mCherry-hLC3 transfected HeLa cell. For live-cell imaging, chamber was maintained at 37 ℃, 5% CO_2 condition. Before imaging, LDs were stained with SF44 (10 μM) for 30 m. Image was obtained with 100× scale, using mCherry/mCherry, CFP/YFP (Excitation/Emission) filter sets. mCherry (excitation: 575/25 nm, emission: 625/45 nm); and CFP/YFP (excitation: 438/24 nm, emission: 559/38 nm). Images were analyzed with SoftWorks deconvolution software.

Lysosome and LD imaging HeLa cells were seeded on Lab-Tek II Chambered Coverglass w/Cover #1.5 Borosilicate Sterile/8 Well

(Nunc 155409). DeltaVision Elite imaging system was used for the imaging. For live-cell imaging, chamber was maintained at 37 ℃, 5% CO_2 condition. Before imaging, lysosomes were stained with Lysotracker DeepRed (50 μM, Thermo Scientific, L7528) for 1.5 h, LDs were stained with SF44 (10 μM) for 30 m and nucleus were stained with Hoechst 33342 (2 μg/ml) for 30 m. Images were obtained with 100× scale, using Cy5/Cy5, FITC/TRITC and DAPI/DAPI (Excitation/Emission) filter sets. Cy5 (excitation: 632/22 nm, emission: 676/34 nm); and FITC/TRITC (excitation: 475/28 nm, emission: 594/45 nm); and DAPI/DAPI (excitation: 380/18 nm, emission: 435/48 nm). Images were analyzed with SoftWorks deconvolution software.

Immunofluorescence Hep G2 cells were seeded on Lab-Tek II Chambered Coverglass w/Cover #1.5 Borosilicate Sterile/8 Well (Nunc 155409) and incubated at 37 ℃ for overnight. After incubation with indicated time and concentration of compounds, cells were washed with cold PBS and fixed with 3.7% formaldehyde in PBS. For the permeabilization, cells were incubated in 0.1% Triton X-100 in PBS for 15 min at room temperature. The resulting cells were washed with ice-cold PBS for three times, followed by the incubation with 3% BSA in PBS for 1 h at room temperature. Fixed cells on dish were exposed to the diluted primary antibody solution (ubiquitin (ab7780); 1:300) in PBS with 1% BSA at 4 ℃ for overnight. Primary antibody

was decanted and washed with PBS for three times. Then, a diluted secondary antibody solution (1:200) of secondary antibody, conjugated with TRITC fluorescent dye, was added and the resulting samples were incubated at room temperature in dark for 1 h. After washing by PBS 3 times, fluorescence images were taken in PBS condition using DeltaVision Elite fluorescence microscopy.

RT-PCR Total RNA was isolated from cell cultures using the RNeasy Plus mini kit (Qiagen 74134). Reverse transcription reaction was performed with AccuPower Cycle Script RT PreMix (Bioneer K-2044). For quantitative RT-PCR (qPCR), reactions were performed with KAPA SYBR FAST ABI Prime (KK4605). All qPCR reactions were run at 40 cycles.

Table. 3.1. RT-PCR primers

Genes	Primer sequences
atf4	Forward 5'-GTTCTCCAGCGACAAGGCTA-3' Reverse 5'-ATCCTGCTTGCTGTTGTTGG-3'
chop	Forward 5'-AGAACCAGGAAACGGAAACAGA-3' Reverse 5'-TCTCCTTCATGCGCTGCTTT-3'
spliced xbp1	Forward 5'-CTGAGTCCGAATCAGGTGCAG-3' Reverse 5'-ATCCATGGGGAGATGTTCTGG-3'
p62	Forward 5'-GTGGTAGGAACCCGCTACAA-3' Reverse 5'-GCGATCTTCCTCATCTGCTC-3'
gapdh	Forward 5'-AGGGCTGCTTTTAACTCTGGT-3' Reverse 5'-CCCCACTTGATTTTGGAGGGA-3'

3.3. Results and Discussion

3.3.1. Image-based LD-monitoring high-contents screening and Hit compound selection

The one of the excellent system which is monitoring LD with a specific LD staining fluorescent dye, SF44, in image-based high-throughput manner was developed in Park's group. Using the LD monitoring screening system, about 2000 in-house library compound's LD modulation activity was checked on HeLa cell line at 10 μM concentration. Quite toxic compounds and crystalized compounds in media were excluded from the captured images. Screening results are presented on a heat map (Fig. 3.1). Based on the DMSO control as a

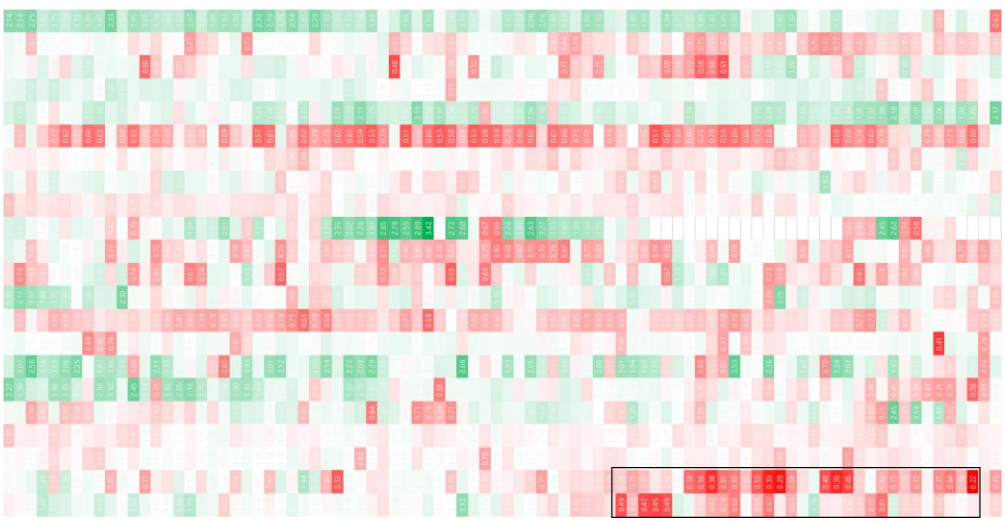

Figure 3.1. Image-based LD monitoring high-contents screening results. HeLa cells were treated with in-house library compounds at 10 μM for 24 h. LDs counts upon treatment with compounds are normalized over DMSO control.

normalization standard, red color-corded indicates LD reduction activity and green color-corded means LD increase. In this study, I focused on a LD reduction mechanism, therefore, boxed compounds group in Fig. 3.1 were selected as a primary hit compound group.

The primary hit compounds were from the same library. The library was deigned to three parts. With triazole or isoxazole as the center linker, core structures such as indole, benzopyran, quinoline and pyrimidine, were attached on left side and alkyl or aryl part were attached on right side (Fig. 3.2). LD reduction activity was evaluated dose-dependently about the primary hit compounds for confirmation of precise activity and for structure and activity relationship study. From the experiments, regardless of center linker, 2-hydroxy quinolone substituted compounds on the left side and ortho-methoxy

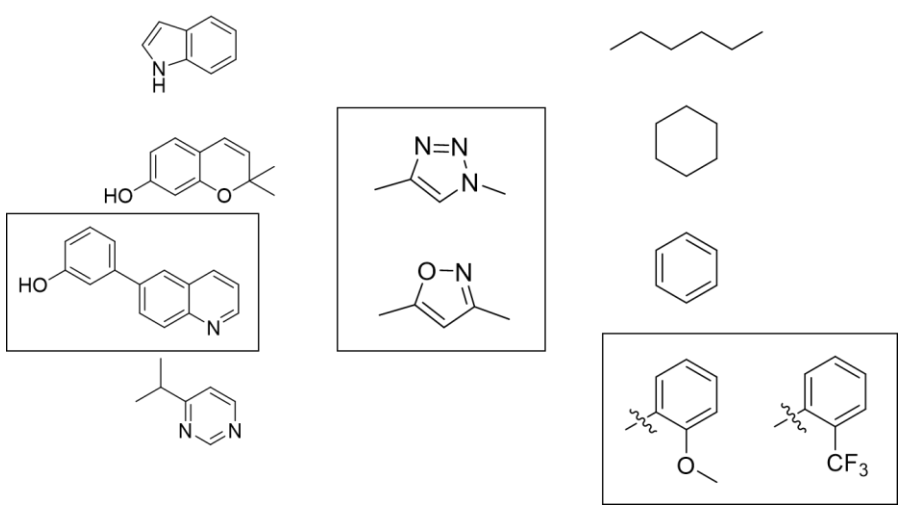

Figure 3.2. Structure and relationship pattern. Regardless of center triazole or isoxazole, hydroxy quinolone substituted compounds on the left side and ortho-methoxy phenyl or tri-fluoromethyl phenyl substituted compounds on the right side showed LDs reducing activity.

phenyl or tri-fluoromethyl phenyl substituted compounds on the right side showed LDs reducing activity dose-dependently. Finally, we selected the most potent compound, **SB2301** as a final hit compound.

SB2301 showed dose-dependent LD reduction activity with IC_{50} 5 μM and on viability assay, the compound showed mild cytotoxicity with IC_{50} 15 μM on HeLa cell line upon 48 h treatment (Fig. 3.3).

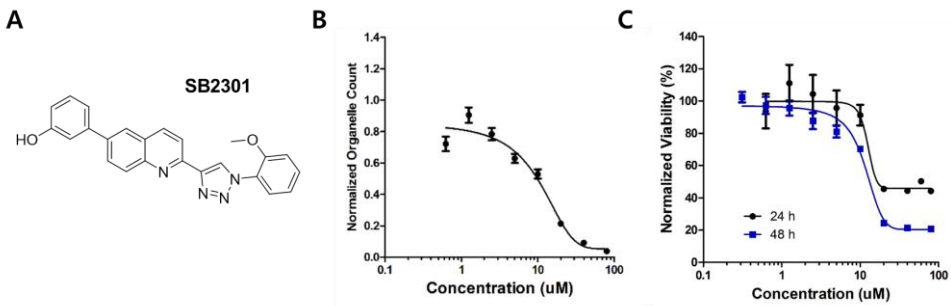

Figure 3.3 Hit compound, **SB2301**. (A) Compound structure (B) LD reduction activity on HeLa cell for 24 h treatment (C) Cell viability for 24 h or 48 h.

3.3.2. Selective autophagy, especially lipophagy activation

I tested whether it activated autophagy process or not. LC3 protein is one of the autophagy process markers. LC3 I protein is lapidated to LC3 II protein on phagophore surface when autophagy proceeds. In western blotting analysis, LC3 I changes to LC3 II was observed upon **SB2301** treatment in dose-dependent and in time-course study (Fig. 3.4A and B). Further, autophagic flux was measured by **SB2301** and Bafilomycin A1 (Baf) combination treatment [72]. Baf is a known inhibitor of vacuolar-type H^+-ATPase, which inhibits the

autolysosomal degradation of cellular contents as well as autophagosomal-lysosomal fusion through the inhibition of acidification, thereby blocking the late-stage flux of autophagy. As shown in Fig. 3.4C, treatment Baf with **SB2301** made LC3 II conversion much stronger. It signified autophagy process was activated and autophagy full flux went ahead by the compound. To cross confirm full autophagic flux in live cell condition, mcherry-GFP-LC3 protein imaging experiment was carried out. Owing to the intrinsic quenching property of GFP in acidic condition, it is possible to differentiate autophagosomes (neutral) and autolysosomes (acidic) by LC3 fused fluorescence protein signal changes. Upon Rapamycin treatment, autophagy process was activated by inhibiting mTORC1 and GFP signal was quenched. In contrast, in Baf condition, it neutralized lysosomal acidification and arrested autophagic flux and, then, GFP signal was maintained. In comparison with control conditions, **SB2301** made GFP signal quenched like Rapamycin (Fig. 3.4D). It indicated that autophagic flux carried on like Rapamycin and supported to previous western blotting analysis.

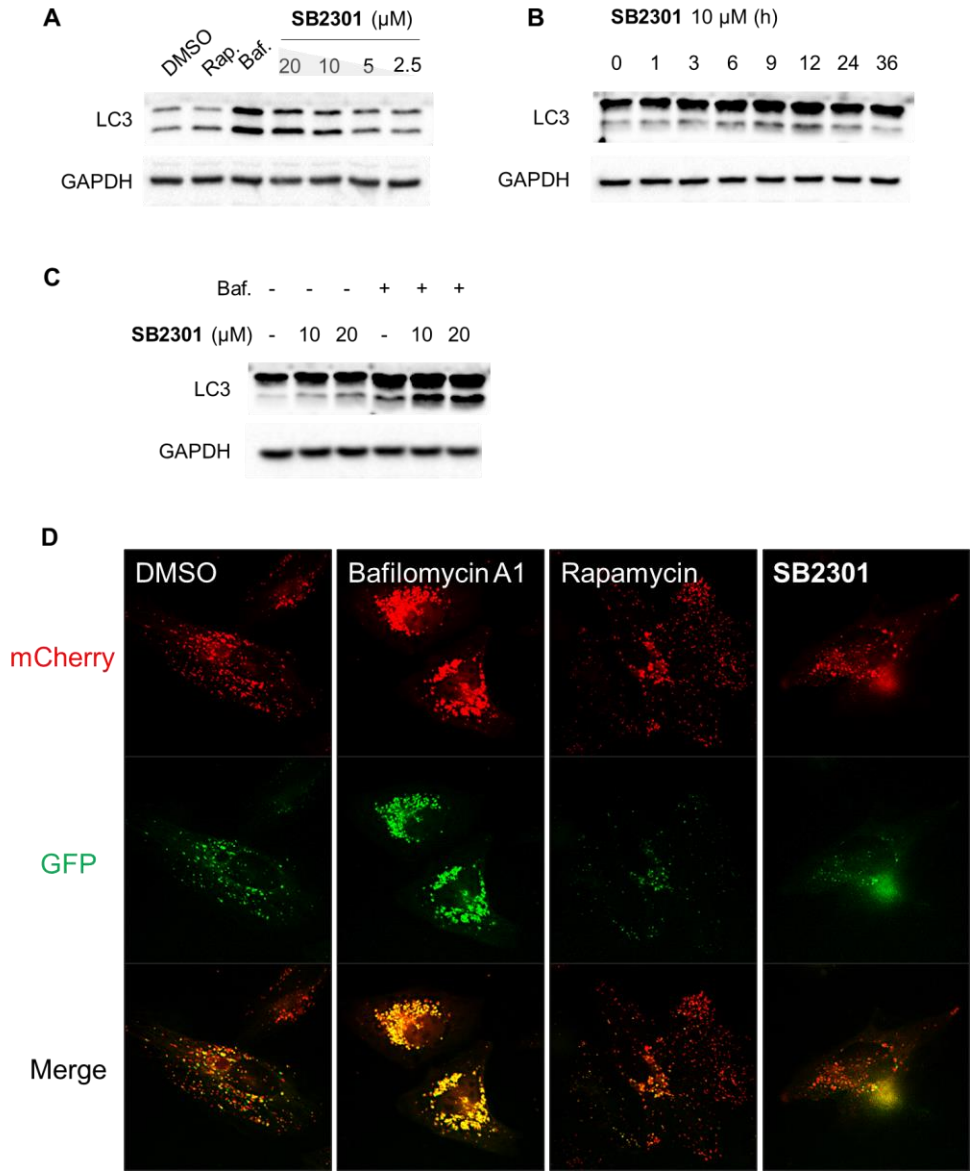

Figure 3.4. Autophagy activation by **SB2301** (A) Hep G2 cells were treated with **SB2301** for 12 h at various concentration (B) Hep G2 cells were treated with **SB2301** 10 μM in time-course. (C) Hep G2 cells were treated with **SB2301** and Bafilomycin A1 5 nM for 6 h. (D) HeLa cells were transfected with mCherry-GFP-LC3 plasmid and treated with 500 nM of Rap, 20 nM of Baf or 5 μM of **SB2301** for 16 h.

To confirm the usage of LD as an autophagy substrate, locations of LD and autophagosome/autolysosome were observed. First, LD and LC3 protein monitoring was performed on mCherry-LC3 protein expressing cells in live cell condition. As shown in Fig. 3.5A, no changes of LC3 and LD quantities were observed and part of LC3 proteins and LDs were fused together upon DMSO or Rapamycin treatment. In contrast, Chloroquine, lysosome acidification inhibitor like Bafilomycin A1, made LD accumulate and we could observe more LC3 proteins and LD colocalization than DMSO. In the **SB2301** treatment condition, decreased LD and increased LC3 signals were observed. It signified that 1) more autophagosomes were formed following an autophagy activation and 2) whole or partial LD was sequestered in autophagosomes by **SB2301**. These sequestered LDs were eventually fused with lysosomes involving to hydrolyze LD (Fig. 3.5B). These serial experiments demonstrated that **SB2301** induced the selective autophagy to LD, called lipophagy.

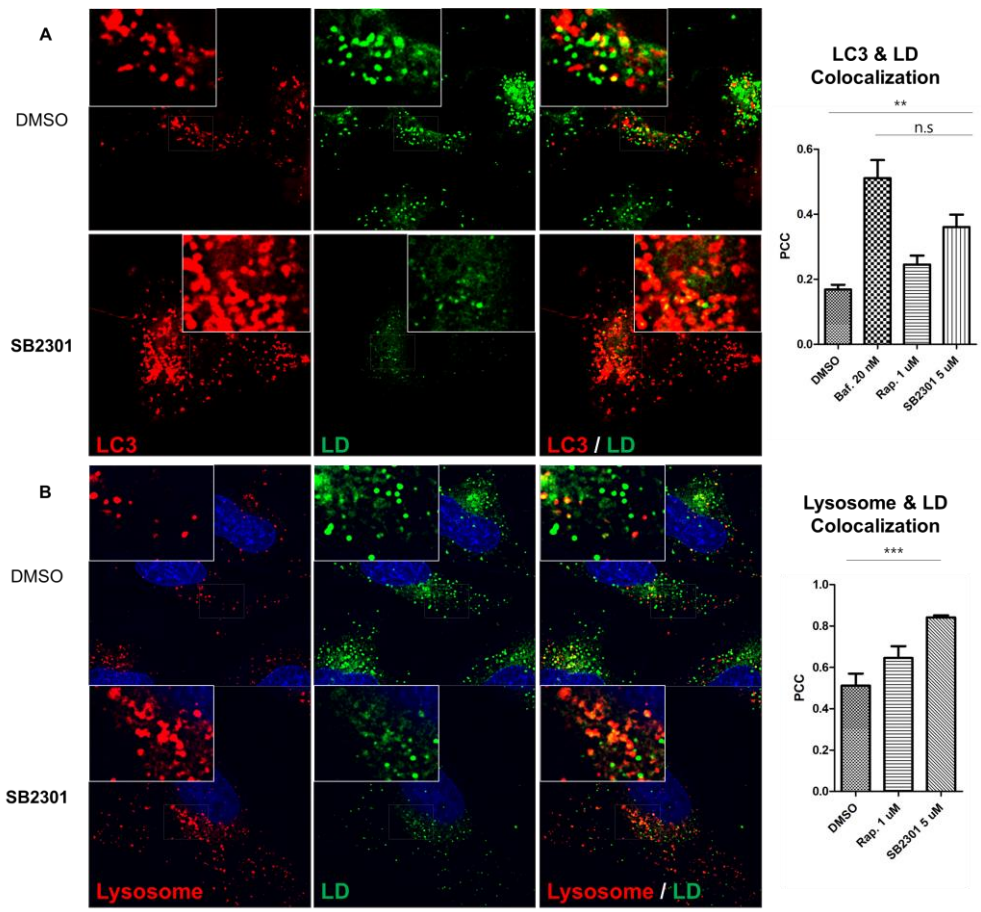

Figure 3.5. Lipophagy activation by **SB2301**. (A) HeLa cells were transfected with mCherry-LC3 plasmid and treated with **SB2301** 5 μM for 12 h. LDs were stained with SF44 for 30 m before imaging and images were captured in live cell condition. (B) HeLa cells were treated with **SB2301** 5 μM for 12 h. LDs were stained with SF44 for 30 m and lysosomes were stained with Lysotracker DeepRed for 1.5 h before imaging and images were captured in live cell condition.

3.3.3. Ubiquitination of LD surface proteins

To assess implications of ubiquitin-mediated mechanism to lipophagy, I performed immunofluorescence imaging. Interestingly, a lot of ubiquitinated proteins decorated the LD surface in **SB2301** condition compared to in DMSO condition (Fig. 3.6). Meanwhile, increase of ubiquitinated protein level even in cytoplasm besides LD surface was observed in western blotting analysis and immunofluorescence imaging experiments. Then, cytoplasmic ubiquitin signals were subtracted as background signal and I calculated the fluorescent signal ratio (Ubiquitin/LD). As a result, ratio of ubiquitin over LD signal was higher in **SB2301** condition (Fig. 3.6). That is, LD surface proteins were ubiquitinated more selectively than cytoplasmic proteins.

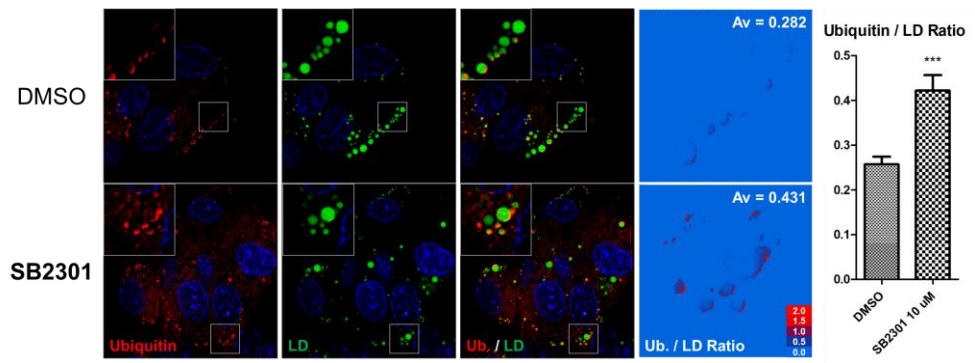

Figure 3.6 Ubiquitination on LD. Hep G2 cells were treated with **SB2301** 10 μM for 12 h. Cells were fixed and immunostained with ubiquitin antibody. Fixed LDs were stained BODIPY 493/503. LD intensity over ubiquitin intensity ratio was calculated after subtraction of cytoplasmic ubiquitin signals as background signals.

The first cue to degrade ubiquitinated substrate is ubiquitin-proteasome system (UPS). However, autophagy-lysosome system is also used for clearance including ubiquitinated aggregates or organelles which is not appropriate substrate of proteasomes. Therefore, it should be differentiated on the case of ubiquitinated LDs. On LD monitoring system, proteasome inhibitor, MG132 or Bortezomib could not reduce LD and **SB2301** maintained its LD reduction activity even with MG132 or Bortezomib (Fig. 3.7). It demonstrated **SB2301** activity was independent to proteasomal degradation. It might result from LD's hydrophobicity.

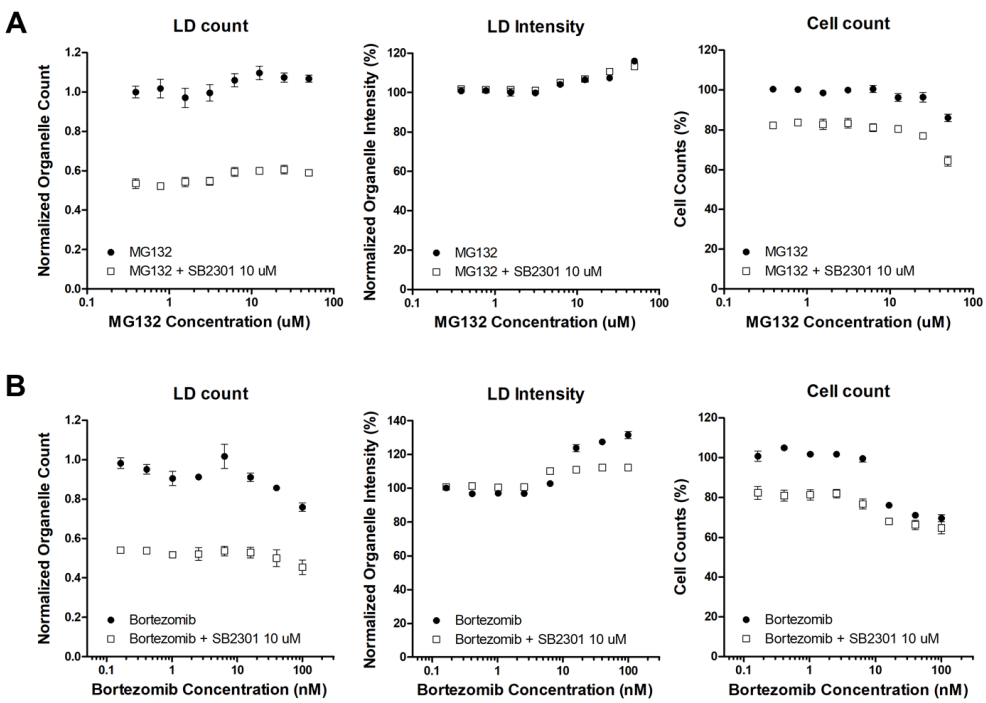

Figure 3.7. Orthogonal LD reduction mechanism to proteasomal inhibition. Hep G2 were treated with (A) MG132 or (B) Bortezomib with or without **SB2301** 10 μM for 24 h. LD count, intensity and cell numbers are quantified.

3.3.4. Relationship with Endoplasmic reticulum (ER) stress

For studying how LD surface proteins are ubiquitinated and how autophagy process is activated, it is necessary to understand where LD surface proteins are originated. LD surface proteins can be inserted on LD surface from two distinct pathways [37, 73]. Some proteins are from ER membrane. LD is formed on ER membrane and the nascent LD might remain attached to the ER or separate completely. At this time, hairpin-structural proteins expressed on ER membrane can move to LD. The others are from cytoplasm. Amphiphilic motif bearing proteins synthesized in cytoplasmic ribosome can be inserted directly to LD such as perilipin family proteins. To differentiate the origin of ubiquitinated protein by **SB2301**, ER stress markers were monitored and it is confirmed that **SB2301** induced ER stress in western blotting analysis and RT-PCR (Fig. 3.8). In addition, a unique ubiquitination pattern on LD was observed. As shown in Fig. 3.6, ubiquitinated proteins were located to the outer corner with nucleus as the center. From these two experiments, I inferred that **SB2301** induced ER stress by perturbation of specific machineries related to ubiquitination in ER and make LD proteins ubiquitinate simultaneously. This hypothesis was also supported by ATF4 activation in the next order to activate ER stress associated degradation (ERAD) signaling [74-77].

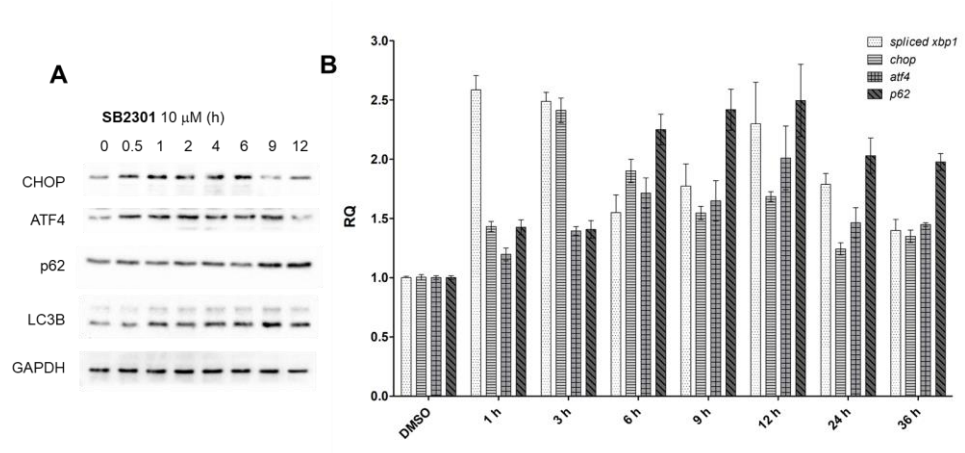

Figure 3.8. ER stress induction. Hep G2 cells were treated with **SB2301** 10 μM for indicated time. (A) CHOP, ATF4, p62, LC3B and GAPDH were determined by western blotting analysis. (B) *spliced xbp1*, *chop*, *atf4* and *p62* mRNA expression level were determined by RT-PCR.

3.3.5. LD reduction in drug induced steatosis *in vitro* model

As an aspect of drug discovery, LD reduction is quite fascinating phenotype because LD accumulation is engaged in many metabolic diseases such as type 2 diabetes and steatohepatitis. Therefore, I tested whether the compound could attenuate steatosis or not in drug-induced steatosis model. Two control compounds were chosen for the steatosis inducer, oleic acid (OA) as a simple high-fat dietary mimic system and Tamoxifen as a more severe steatohepatitis mimic system. Fortunately, **SB2301** showed LD reduction effects in both steatosis models (Fig. 3.9). Upon treatment OA, LD number, size and fluorescence intensity all increased and **SB2301** reduced LD's size

and area dose-dependently even with OA. In the case of Tamoxifen, it made LD more intense and **SB2301** also reduced its size and area dose-dependently.

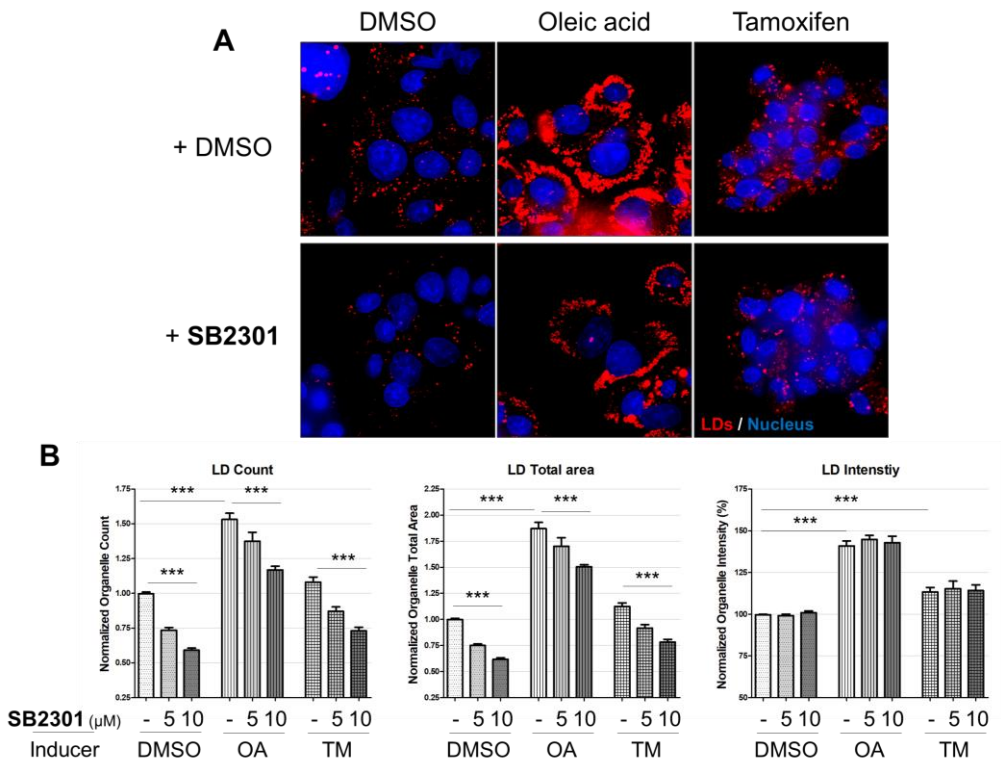

Figure 3.9. LD reduction in drug induced steatosis *in vitro* model. Hep G2 cells were treated with oleic acid (OA) 75 μM or Tamoxifen (TM) 10 μM for 24 h for inducing steatosis followed by **SB2301** 5 or 10μM for 24 h with each inducer. LDs were stained with SF44 for 30 m before imaging and images were captured in live cell condition. (B) Representative images from imaging conducted by DeltaVision Elite. (B) Quantification of the imaging results conducted by InCell Analyzer 2000. LD count, total area and intensity were quantified by InCell Developer software.

3.4. Conclusion

Lipid droplet (called LD) is a specialized organelle used for cellular free fatty acid storage as a neutral lipid form such as triacylglycerol or sterol esters for efficient lipid storage and avoiding lipotoxicity of free fatty acid. LD plays an important role in energy homeostasis and lipid metabolisms by changing its forms over their environment such as tissue types and energy conditions. LD research field have been emerged as a major interest because of its importance in biological and physiological systems in both academic and industrial field though its limited information and research pools.

With a chemical biology perspective, I desired to approach this research field with a bioactive small molecule modulating LD. To identify a bioactive small molecule, image-based LD monitoring high-contents screening system was conducted because 1) LD itself is regarded as a good phonotype representing cellular metabolic states, 2) it is not restrained the limited information and 3) it is possible to approach unbiased and varied manner, which allows opportunities to identify novel LD modulation mechanisms.

The most potent LD reducing compound **SB2301** activates LD's clearance mechanism via autophagy process, lipophagy and this mechanism was mediated by ubiquitination of LD proteins. Finally, **SB2301** showed LD reduction effects in oleic acid or Tamoxifen induced steatosis models. Even though there are limited information

of LD, I approached the mode of action with proper cellular imaging experiments.

Ubiquitination mediated selective autophagy have been reported but in the case of LD, it has been guessed to be the similar mechanisms. Therefore, I expect to investigate a novel LD reduction mechanism to extend LD regulation comprehension and to suggest non-alcoholic steatohepatitis (NASH) attenuation strategy through the investigated mechanism of **SB2301**.

References

1. Terstappen, G.C., et al., *Target deconvolution strategies in drug discovery.* Nature Reviews Drug Discovery, 2007. **6**: p. 891.
2. Kubota, K., M. Funabashi, and Y. Ogura, *Target deconvolution from phenotype-based drug discovery by using chemical proteomics approaches.* Biochimica et Biophysica Acta (BBA) - Proteins and Proteomics, 2019. **1867**(1): p. 22-27.
3. Gonzalez-Munoz, A.L., R.R. Minter, and S.J. Rust, *Phenotypic screening: the future of antibody discovery.* Drug Discovery Today, 2016. **21**(1): p. 150-156.
4. Jo, A., et al., *A high-content screening platform with fluorescent chemical probes for the discovery of first-in-class therapeutics.* Chem Commun (Camb), 2016. **52**(47): p. 7433-45.
5. Lee, S., E. Kim, and S.B. Park, *Discovery of autophagy modulators through the construction of a high-content screening platform via monitoring of lipid droplets.* Chemical Science, 2013. **4**(8): p. 3282-3287.
6. Kim, E., S. Lee, and S.B. Park, *A Seoul-Fluor-based bioprobe for lipid droplets and its application in image-based high throughput screening.* Chemical Communications, 2012. **48**(17): p. 2331-2333.
7. Hegyi, J. and V. Hegyi, *Chapter 9 - New Developments in Fluorescence Diagnostics*, in *Imaging in Dermatology*, M.R.

Hamblin, P. Avci, and G.K. Gupta, Editors. 2016, Academic Press: Boston. p. 89-94.

8. Heeres, J.T. and P.J. Hergenrother, *High-throughput screening for modulators of protein-protein interactions: use of photonic crystal biosensors and complementary technologies.* Chemical Society Reviews, 2011. **40**(8): p. 4398-4410.
9. Szollosi, J., S. Damjanovich, and L. Matyus, *Application of fluorescence resonance energy transfer in the clinical laboratory: routine and research.* Cytometry, 1998. **34**(4): p. 159-79.
10. Broussard, J.A., et al., *Fluorescence resonance energy transfer microscopy as demonstrated by measuring the activation of the serine/threonine kinase Akt.* Nat Protoc, 2013. **8**(2): p. 265-81.
11. Piston, D.W. and G.J. Kremers, *Fluorescent protein FRET: the good, the bad and the ugly.* Trends Biochem Sci, 2007. **32**(9): p. 407-14.
12. Jewell, J.L. and K.L. Guan, *Nutrient signaling to mTOR and cell growth.* Trends Biochem Sci, 2013. **38**(5): p. 233-42.
13. Laplante, M. and D.M. Sabatini, *mTOR signaling in growth control and disease.* Cell, 2012. **149**(2): p. 274-93.
14. Ballou, L.M. and R.Z. Lin, *Rapamycin and mTOR kinase inhibitors.* J Chem Biol, 2008. **1**(1-4): p. 27-36.
15. Efeyan, A. and D.M. Sabatini, *Nutrients and growth factors in mTORC1 activation.* Biochem Soc Trans, 2013. **41**(4): p. 902-5.

16. Dibble, C.C. and B.D. Manning, *Signal integration by mTORC1 coordinates nutrient input with biosynthetic output.* Nat Cell Biol, 2013. **15**(6): p. 555-564.
17. Easton, J.B. and P.J. Houghton, *mTOR and cancer therapy.* Oncogene, 2006. **25**(48): p. 6436-46.
18. Liu, Q., et al., *mTOR Mediated Anti-Cancer Drug Discovery.* Drug Discov Today Ther Strateg, 2009. **6**(2): p. 47-55.
19. Haissaguerre, M., N. Saucisse, and D. Cota, *Influence of mTOR in energy and metabolic homeostasis.* Mol Cell Endocrinol, 2014. **397**(1-2): p. 67-77.
20. Chiarini, F., et al., *Current treatment strategies for inhibiting mTOR in cancer.* Trends in Pharmacological Sciences, 2015. **36**(2): p. 124-135.
21. Benjamin, D., et al., *Rapamycin passes the torch: a new generation of mTOR inhibitors.* Nat Rev Drug Discov, 2011. **10**(11): p. 868-880.
22. Yoon, S.O. and P.P. Roux, *Rapamycin resistance: mTORC1 substrates hold some of the answers.* Curr Biol, 2013. **23**(19): p. R880-3.
23. Bar-Peled, L. and D.M. Sabatini, *Regulation of mTORC1 by amino acids.* Trends Cell Biol, 2014. **24**(7): p. 400-6.
24. Kim, E., et al., *Regulation of TORC1 by Rag GTPases in nutrient response.* Nat Cell Biol, 2008. **10**(8): p. 935-945.
25. Jewell, J.L., et al., *Differential regulation of mTORC1 by*

leucine and glutamine. Science, 2015. **347**(6218): p. 194-198.

26. Nie, C., et al., *Branched Chain Amino Acids: Beyond Nutrition Metabolism.* Int J Mol Sci, 2018. **19**(4).
27. Lynch, C.J., *Role of Leucine in the Regulation of mTOR by Amino Acids: Revelations from Structure–Activity Studies.* The Journal of Nutrition, 2001. **131**(3): p. 861S-865S.
28. Drummond, M.J., et al., *Nutritional and contractile regulation of human skeletal muscle protein synthesis and mTORC1 signaling.* Journal of Applied Physiology, 2009. **106**(4): p. 1374-1384.
29. Nagasawa, T., et al., *Rapid suppression of protein degradation in skeletal muscle after oral feeding of leucine in rats.* The Journal of Nutritional Biochemistry, 2002. **13**(2): p. 121-127.
30. Han, J.M., et al., *Leucyl-tRNA synthetase is an intracellular leucine sensor for the mTORC1-signaling pathway.* Cell, 2012. **149**(2): p. 410-24.
31. Bonfils, G., et al., *Leucyl-tRNA synthetase controls TORC1 via the EGO complex.* Mol Cell, 2012. **46**(1): p. 105-10.
32. Tsun, Z.Y., et al., *The folliculin tumor suppressor is a GAP for the RagC/D GTPases that signal amino acid levels to mTORC1*. Mol Cell, 2013. **52**(4): p. 495-505.
33. Rebsamen, M., et al., *SLC38A9 is a component of the lysosomal amino acid sensing machinery that controls mTORC1*. Nature, 2015. **519**(7544): p. 477-81.

34. Wang, S., et al., *Lysosomal amino acid transporter SLC38A9 signals arginine sufficiency to mTORC1.* Science, 2015. **347**(6218): p. 188-194.

35. Wolfson, R.L., et al., *Sestrin2 is a leucine sensor for the mTORC1 pathway.* Science, 2016. **351**(6268): p. 43-48.

36. Thiam, A.R., R.V. Farese Jr, and T.C. Walther, *The biophysics and cell biology of lipid droplets.* Nat Rev Mol Cell Biol, 2013. **14**(12): p. 775-786.

37. Bersuker, K. and J.A. Olzmann, *Establishing the lipid droplet proteome: Mechanisms of lipid droplet protein targeting and degradation.* Biochimica et Biophysica Acta (BBA) - Molecular and Cell Biology of Lipids, 2017. **1862**(10, Part B): p. 1166-1177.

38. Welte, M.A., *Expanding roles for lipid droplets.* Curr Biol, 2015. **25**(11): p. R470-81.

39. Pol, A., S.P. Gross, and R.G. Parton, *Biogenesis of the multifunctional lipid droplet: Lipids, proteins, and sites.* The Journal of Cell Biology, 2014. **204**(5): p. 635-646.

40. Meyers, A., T.M. Weiskittel, and P. Dalhaimer, *Lipid Droplets: Formation to Breakdown.* Lipids, 2017. **52**(6): p. 465-475.

41. Ben M'barek, K., et al., *ER Membrane Phospholipids and Surface Tension Control Cellular Lipid Droplet Formation.* Developmental Cell, 2017. **41**(6): p. 591-604.e7.

42. Schulze, R.J., A. Sathyanarayan, and D.G. Mashek, *Breaking*

fat: The regulation and mechanisms of lipophagy. Biochimica et Biophysica Acta (BBA) - Molecular and Cell Biology of Lipids, 2017. **1862**(10, Part B): p. 1178-1187.

43. Zechner, R., F. Madeo, and D. Kratky, *Cytosolic lipolysis and lipophagy: two sides of the same coin.* Nature Reviews Molecular Cell Biology, 2017. **18**(11): p. 671-684.
44. Singh, R. and A.M. Cuervo, *Lipophagy: connecting autophagy and lipid metabolism.* Int J Cell Biol, 2012. **2012**: p. 282041.
45. Cuervo, A.M., *Autophagy: Many paths to the same end.* Molecular and Cellular Biochemistry, 2004. **263**(1): p. 55-72.
46. Mizushima, N., *Autophagy: process and function.* Genes & Development, 2007. **21**(22): p. 2861-2873.
47. Rogov, V., et al., *Interactions between Autophagy Receptors and Ubiquitin-like Proteins Form the Molecular Basis for Selective Autophagy.* Molecular Cell, 2014. **53**(2): p. 167-178.
48. Sica, V., et al., *Organelle-Specific Initiation of Autophagy.* Molecular Cell, 2015. **59**(4): p. 522-539.
49. Geisler, S., et al., *PINK1/Parkin-mediated mitophagy is dependent on VDAC1 and p62/SQSTM1*. Nature Cell Biology, 2010. **12**: p. 119.
50. Kim, P.K., et al., *Ubiquitin signals autophagic degradation of cytosolic proteins and peroxisomes.* Proceedings of the National Academy of Sciences, 2008. **105**(52): p. 20567-20574.
51. Singh, R., et al., *Autophagy regulates lipid metabolism.* Nature,

2009. **458**(7242): p. 1131-1135.

52. Ward, C., et al., *Autophagy, lipophagy and lysosomal lipid storage disorders.* Biochimica et Biophysica Acta (BBA) - Molecular and Cell Biology of Lipids, 2016. **1861**(4): p. 269-284.

53. Gatica, D., V. Lahiri, and D.J. Klionsky, *Cargo recognition and degradation by selective autophagy.* Nature Cell Biology, 2018. **20**(3): p. 233-242.

54. Matsumoto, G., et al., *Serine 403 Phosphorylation of p62/SQSTM1 Regulates Selective Autophagic Clearance of Ubiquitinated Proteins.* Molecular Cell, 2011. **44**(2): p. 279-289.

55. Kaur, J. and J. Debnath, *Autophagy at the crossroads of catabolism and anabolism.* Nat Rev Mol Cell Biol, 2015. **16**(8): p. 461-472.

56. Onal, G., et al., *Lipid Droplets in Health and Disease.* Lipids in Health and Disease, 2017. **16**(1): p. 128.

57. Gluchowski, N.L., et al., *Lipid droplets and liver disease: from basic biology to clinical implications.* Nature Reviews Gastroenterology &Amp; Hepatology, 2017. **14**: p. 343.

58. Vignot, S., et al., *mTOR-targeted therapy of cancer with rapamycin derivatives.* Ann Oncol, 2005. **16**(4): p. 525-37.

59. Houghton, S.H.a.P.J., *Resistance to rapamycin: A novel anticancer drug.* Cancer and Metastasis Reviews, 2001.

60. Choo, A.Y. and J. Blenis, *Not all substrates are treated equally: Implications for mTOR, rapamycin-resistance, and cancer therapy.* Cell Cycle, 2009. **8**(4): p. 567-572.

61. Choo, A.Y., et al., *Rapamycin differentially inhibits S6Ks and 4E-BP1 to mediate cell-type-specific repression of mRNA translation.* Proceedings of the National Academy of Sciences, 2008. **105**(45): p. 17414-17419.

62. Gruppuso, P.A., J.M. Boylan, and J.A. Sanders, *The physiology and pathophysiology of rapamycin resistance.* Cell Cycle, 2011. **10**(7): p. 1050-1058.

63. Yang, H., R. Gong, and Y. Xu, *Control of cell growth: Rag GTPases in activation of TORC1*. Cell Mol Life Sci, 2013. **70**(16): p. 2873-85.

64. Jewell, J.L., R.C. Russell, and K.-L. Guan, *Amino acid signalling upstream of mTOR.* Nat Rev Mol Cell Biol, 2013. **14**(3): p. 133-139.

65. Kim, C., et al., *beta-Turn mimetic-based stabilizers of protein-protein interactions for the study of the non-canonical roles of leucyl-tRNA synthetase.* Chem Sci, 2016. **7**(4): p. 2753-2761.

66. Giordanetto, F., A. Schafer, and C. Ottmann, *Stabilization of protein-protein interactions by small molecules.* Drug Discov Today, 2014. **19**(11): p. 1812-21.

67. Kim, J., et al., *Diversity-oriented synthetic strategy for developing a chemical modulator of protein-protein interaction.*

Nat Commun, 2016. **7**: p. 13196.

68. Hara, K., et al., *Regulation of eIF-4E BP1 Phosphorylation by mTOR.* Journal of Biological Chemistry, 1997. **272**(42): p. 26457-26463.

69. Kim, J., et al., *AMPK and mTOR regulate autophagy through direct phosphorylation of Ulk1*. Nat Cell Biol, 2011. **13**(2): p. 132-41.

70. Mondesire, W.H., et al., *Targeting Mammalian Target of Rapamycin Synergistically Enhances Chemotherapy-Induced Cytotoxicity in Breast Cancer Cells.* Clinical Cancer Research, 2004. **10**(20): p. 7031-7042.

71. Walther, T.C. and R.V. Farese, Jr., *Lipid droplets and cellular lipid metabolism.* Annu Rev Biochem, 2012. **81**: p. 687-714.

72. Klionsky, D.J., et al., *Guidelines for the use and interpretation of assays for monitoring autophagy (3rd edition).* Autophagy, 2016. **12**(1): p. 1-222.

73. Kory, N., R.V. Farese, Jr., and T.C. Walther, *Targeting Fat: Mechanisms of Protein Localization to Lipid Droplets.* Trends in Cell Biology, 2016. **26**(7): p. 535-546.

74. Ogata, M., et al., *Autophagy Is Activated for Cell Survival after Endoplasmic Reticulum Stress.* Molecular and Cellular Biology, 2006. **26**(24): p. 9220-9231.

75. Rashid, H.O., et al., *ER stress: Autophagy induction, inhibition and selection.* Autophagy, 2015. **11**(11): p. 1956-1977.

76. Senft, D. and Z.A. Ronai, *UPR, autophagy, and mitochondria crosstalk underlies the ER stress response.* Trends Biochem Sci, 2015. **40**(3): p. 141-8.

77. B'Chir, W., et al., *The eIF2alpha/ATF4 pathway is essential for stress-induced autophagy gene expression.* Nucleic Acids Res, 2013. **41**(16): p. 7683-99.

국 문 초 록

생리활성 저분자 화합물의 발굴과 세포 이미징을 통한 작용 기전의 이해

정 진 주

서울대학교 대학원

생물물리 및 화학생물학과 화학생물학 전공

우리 몸은 항상성을 유지하기 위한 매우 정교하고 복잡한 신호전달체계를 갖추고 있다. 그러므로, 생체 내 현상을 조절하는 작용 원리를 연구하면 인체의 생장 방식을 이해할 수 있고, 이를 바탕으로 질병의 치료 전략을 제시함으로써 인류의 삶의 질을 높일 수 있다. 새로운 생명 현상을 탐구하고 이해하기 위한 방법은 여러 가지가 있는데, 본 학위 논문에서는 생리활성 저분자 화합물을 발굴하고, 이 화합물의 작용 기전을 세포 이미징을 통해 시각화하여 다양한 측면에서 새로운 생명 현상을 이해하는 화학생물학적 접근 방법을 이용하였다.

본 학위 논문에는 두 가지의 생명 현상을 연구 하였다. 첫 번째는 세포의 성장을 조절하는 중요한 단백질 복합체인 mechanistic target of Rapamycin complex 1 (mTORC1)을 조절할 수 있는 방법 중 하나인 Leucyl-tRNA Synthetase (LRS)와 Ras-like GTPase D (RagD) 단백질 간의 상호작용에 대한 연구이다. 타겟 기반 스크리닝을 통해 서로 다른 세 가지의 LRS-RagD 상호작용 조절 물질을 발굴하고, 각각의 화합물이 일으키는 독특한 활성 변화 양상과 생물물리학 연구 결과를 바탕으로 LRS-RagD 단백질간 상호작용을 통한 mTORC1를 조절하는 새로운 관점에 대해 기술하고 있다. 두 번째는 지방 대사에 중요한 세포 소기관인 지방 방울을 감소 시키는 방법에 대한 내용이다. 이미징 기반 스크리닝을 수행하여 지방 방울을 감소시키는 저분자 화합물을 발굴하고, 이 화합물의 작용 기전을 탐구하여 기존에 보고되지 않은 지방 방울을 줄이는 새로운 작용 기전을 연구한 내용을 기술하고 있다.

LRS-RagD에 의한 mTORC1의 조절 방법과 지방 방울의 감소 작용 기전에 대한 연구는 상대적으로 연구가 미약한 분야이므로 본 학위 논문에 기술된 새로운 연구 결과는 학문적으로 기여하는 바가 크다. 더 나아가, 새로 밝혀진 연구 결과를 바탕으로 새로운 질병 치료 전략을 제시할 수 있는 가능성을 확인하였으므로, 항암 증감제와 지방증 완화제로서의 의약 산업에 적용을 기대하고 있다.

주요어 : 화학 생물학, 생리활성 저분자 화합물, 작용 기전 이해, 세포 이미징, LRS-RagD 상호작용, 지방 방울

학 번 : 2012-23917